

Alleviating the H_0 and σ_8 tensions in the interacting cubic covariant Galileon model

Sihem Zabat, Youcef Kehal , and Khireddine Nouicer 

Laboratory of Theoretical Physics and Department of Physics,
Faculty of Exact and Computer Sciences, University of Jijel,
B.P. 98, Ouled Aissa, Jijel 18000, Algeria

E-mail: sihem.zabat@univ-jijel.dz, youcef.kehal@univ-jijel.dz,
khnouicer@univ-jijel.dz

Abstract. The interaction between dark matter and dark energy has become a focal point in contemporary cosmological research, particularly in addressing current cosmological tensions. This study explores the cubic Galileon model's interaction with dark matter, where the interaction potential in the dark sector is proportional to the dark energy density of the Galileon field. By employing dimensionless variables, we transform the field equations into an autonomous dynamical system. We calculate the critical points of the corresponding autonomous systems and demonstrate the existence of a stable de Sitter epoch. Our investigation proceeds in two phases. First, we conduct a detailed analysis of the exact interacting cubic Galileon (ICG) model, derived from the precise solution of the equations of motion. Second, we explore an approximate tracker solution, labeled TICG, assuming a small coupling parameter between dark matter and dark energy. We evaluate the evolution of these models using data from two experiments, aiming to resolve the tensions surrounding H_0 and S_8 . The analysis of the TICG model indicates a preference for a phantom regime and provides a negative coupling parameter in the dark sector at a 68% confidence level. This model also shows that the current tensions regarding H_0 and S_8 are alleviated. Conversely, the ICG model, despite its preference for the phantom regime, is plagued by an excess in today's matter density and a higher expansion rate, easing only the H_0 tension.

Keywords: DE-DM interaction, cubic Galileon model, H_0 and S_8 tensions

ArXiv ePrint: [2305.12155](https://arxiv.org/abs/2305.12155)

Contents

1	Introduction	1
2	ICG on the background	3
2.1	Dynamical system analysis	4
2.2	Analysis of the fixed points eras	7
3	ICG on the perturbed flat space-time	10
3.1	Perturbed energy momentum tensor	10
3.2	Perturbed Einstein equations	13
3.3	Quasi static approximation	14
3.4	Covariant interaction term	15
4	Methodology and data	16
5	Results and discussion	17
6	Conclusions	25
A	RSD and OHD data tables	33

1 Introduction

It goes without saying that the concordance Λ CDM model stands as the prevailing framework used in cosmology to describe the large-scale structure and evolution of the universe. It postulates the existence of a non-baryon cold dark matter (DM) alongside ordinary matter, playing the essential role in explaining the rotation curves of galaxies and the processes of structures formation [1, 2]. Additionally, the Λ CDM model aligns consistently with a wide range of observational data, including the current accelerated expansion of the universe [3–7]. This latter, can be explained in the framework of general relativity (GR) by introducing an exotic fluid with negative pressure known as dark energy (DE) [8], which is often linked to the cosmological constant [9]. Despite its success, the model still face unresolved issues, casting doubt on its validity [10, 11] such as the cosmological constant problem and the coincidence problem. The first one is related to the huge discrepancy between the theoretical value of vacuum energy density Λ predicted by quantum field theories and the experimental value of DE in the universe [12] while the second one revolves around the peculiar observation that the current densities of vacuum energy and matter in the universe are roughly comparable, despite their distinct evolutionary behaviors [13].

In this regard, alternative directions have been followed to address these problems and demystify the origin of DE that can reproduce the late-time acceleration of the universe. A common way consists of modeling the right hand side of Einstein’s equations with specific forms of matter [14]. For instance, scalar fields can be naturally introduced as candidates for DE such as quintessence model [15–19] in which the quintessence field is minimally coupled to gravity and its equation of state (EoS) is no longer a constant but it rather slightly evolves in time [8, 20]. Other dynamical DE models have been proposed including k-essence [21], tachyons [22, 23] and Chaplygin gas [24–26]. On the other hand, a different path postulates

that GR is only accurate at local systems and fails to describe the universe at larger scales and hence it should be modified [27–29]. Scalar-tensor theories [30] represent a compelling approach within the realm of modified gravity to elucidate the mysteries surrounding DE and cosmic inflation. These theories encompass a broader framework than GR incorporating scalar fields as additional degree of freedom alongside the metric. One prominent example is the Galileon models [31] which are a subset of Horndeski theories, and leads to second order field equations even though their Lagrangians contain higher order derivatives of the field [32, 33]. Galileon is a scalar field π that satisfies the Galilean shift symmetry $\partial_\mu\pi \rightarrow \partial_\mu\pi + b_\mu$ in flat space-time [32], while this property is broken in the covariant version [34, 35] when the Lagrangian is extended to curved space-time. Emerging from the decoupling limit of the DGP braneworld [36–38] to avoid ghost modes, the covariant Galileon field and its extended models have sparked extensive research into their phenomenological aspects. This exploration aims to probe their roles in producing a self-accelerating phase and primordial inflation [39–44], or even proposing a self tuning mechanism to alleviate the cosmological constant problem [45, 46]. Galileon theories are usually relevant to the Vainshtein mechanism, where the scalar mode is weakly coupled to the source. Since that the presence of non-linear derivative interactions in the scalar sector allows to screen the extra force mediated by the scalar field on small scales.

Apart from the theoretical challenges mentioned above, another set of problems emerges from cosmological and astrophysical data. In particular, the present value of the Hubble parameter H_0 is estimated by the Cosmic Microwave Background (CMB) constraints and the Planck collaboration as $H_0 = 67.36 \pm 0.54$ km/s/Mpc [7], while local distance ladder measurements from Type Ia supernovae from the 2019 local measurements by SH0ES collaboration (R19) indicate $H_0 = (73.04 \pm 1.04)$ km/s/Mpc [47, 48] reporting a significant tension of $\sim 5\sigma$. An other tension within the concordance model is the inconsistency between CMB and LSS observations, quantified in terms of the $S_8 = \sigma_8 \sqrt{\Omega_m^{(0)}/0.3}$ parameter, where $\Omega_m^{(0)}$ is the present day matter density. Indeed, the Dark Energy Survey Year-3 (DES-Y3) [49] have revealed a 2.5σ tensions with Planck data assuming Λ CDM model. These tensions, appear not attributed to unknown systematic effects but may signal a potential breakdown of the Λ CDM model. In the same spirit, non-gravitationally interacting models between DE and DM were originally introduced to justify the cosmological constant and coincidence problems [50], and they also seem to be effective in alleviating the H_0 [51–62] and σ_8 [62–65] tensions. Inspired by recent approaches, the primary objective of this paper is to explore potential solutions or mitigation for the cosmological tensions involving H_0 and S_8 by incorporating interacting dark energy (DE) with dark matter (DM) within the framework of the cubic covariant Galileon model. We introduce an interaction term expressed as $Q = \alpha H \rho_x$, where H represents the Hubble parameter, ρ_x denotes the energy density of the Galileon field, and α is a dimensionless coupling parameter.

This paper is organized as follows. In Sec. 2, we introduce the Interacting Cubic Covariant Galileon (ICG) model and derive the corresponding field equations, assuming a spatially flat FLRW space-time. We also analyze the existence and stability of fixed points and extract constraints on the DM-DE coupling constant. Sec. 3 is dedicated to studying the evolution of cosmological perturbations in the presence of perfect fluid matter, investigating the behavior of the growth rate of matter perturbations and the gravitational potential in the quasi-static approximation on sub-horizon scales. In Sec. 4, we describe the cosmological data and the methodology used to obtain constraints on model parameters. Sec. 5 presents the cosmological constraints on model parameters for both the exact and tracker solutions using a Monte Carlo Markov Chain (MCMC) approach. We compare these results with

the Λ CDM model and use the corrected frequentist Akaike Information Criterion (AIC_c) to assess whether the ICG model is favored over the Λ CDM model. Finally, our conclusions are presented in Sec. 6.

2 ICG on the background

The action of minimally coupled cubic covariant Galileon field is described by the action [35]

$$S = \int d^4x \sqrt{-g} \left(\frac{M_{\text{Pl}}^2 R}{2} + \frac{1}{2} c_2 \pi_{;\mu} \pi^{;\mu} + \frac{1}{2} \frac{c_3}{M^3} (\nabla \pi)^2 \square \pi + \mathcal{L}_M [g_{\mu\nu}, \{\phi_a\}] \right) \quad (2.1)$$

where M_{Pl}^2 is the reduced Planck mass, $M_{\text{Pl}}^2 = 1/8\pi G$, c_i are constants parameters, M is a constant with dimensions of mass, and \mathcal{L}_M is the matter Lagrangian.

Varying the action (2.1) with respect to $g_{\mu\nu}$ we obtain the Einstein's field equations:

$$M_{\text{Pl}}^2 G_{\alpha\beta} = \sum_{i=2}^3 c_i T_{\alpha\beta}^{(i)} + \sum_A T_{\alpha\beta}^{(A)}, \quad (2.2)$$

where $G_{\alpha\beta}$ denotes the Einstein symmetric tensor, and

$$T_{\alpha\beta}^{(2)} = -\pi_{;\alpha} \pi_{;\beta} + \frac{1}{2} g_{\alpha\beta} (\nabla \pi)^2, \quad (2.3)$$

$$T_{\alpha\beta}^{(3)} = -\frac{1}{M^3} \left(\pi_{;\alpha} \pi_{;\beta} \square \pi + g_{\alpha\beta} \pi_{;\mu} \pi^{;\mu\lambda} \pi_{;\lambda} - \pi^{;\mu} [\pi_{;\alpha} \pi_{;\beta\mu} + \pi_{;\beta} \pi_{;\alpha\mu}] \right), \quad (2.4)$$

are the contributions to the Galileon energy-momentum tensor, and $T_{\alpha\beta}^{(A)}$ is the energy-momentum tensor of radiation, baryon matter and dark matter ($A = r, b, c$). For matter components, we assume the usual energy-momentum tensor describing a perfect fluid

$$T_{\alpha\beta}^{(A)} = (\rho_A + p_A) u_{\alpha}^A u_{\beta}^A + p_A g_{\alpha\beta}, \quad (2.5)$$

where ρ_A is the energy density, p_A the pressure, and u_{α}^A the velocity of the A -fluid. In order to preserve the local energy-momentum conservation law, the Bianchi identities imply that

$$\nabla_{\alpha} T^{\alpha\beta} = 0. \quad (2.6)$$

In the absence of coupling between matter and energy species we have $\nabla_{\alpha} T^{\alpha\beta(A)} = 0$, which is the case for standard model of particles [66]. In order to study the covariant Galileon model in its generality and allow to the existence of energy transfer between DM and DE as supported by observations of galaxy clusters [67], we assume that the dark sectors do not evolve separately but interact with each other. The usual way to describe this interaction is to introduce an energy-momentum exchange current into the conservation equations as follows

$$\nabla_{\alpha} T_x^{\alpha\beta} = -\nabla_{\alpha} T_c^{\alpha\beta} = Q^{\beta}, \quad (2.7)$$

where Q^{β} is given covariantly by (see [68] and references therein)

$$Q_{x/c}^{\beta} = Q u^{\beta}, \quad (2.8)$$

u^{β} is the DE/DM 4-velocity and Q is the interaction function between DE and DM, and generally it is a function of DE and DM densities, the Hubble parameter and its derivatives. Assuming that there is only energy transfer between DE and DM we have $Q_x = -Q_c = Q$. In this study we are interested by the case $Q \sim \rho_x$, where positive Q indicates that DM decays to DE, whereas DE decays to DM for negative Q .

2.1 Dynamical system analysis

To study the background cosmological dynamics of the ICG, we assume the geometry of spatially flat expanding universe described by the FLRW metric

$$ds^2 = -n^2(t) dt^2 + a^2(t) \delta_{ij} dx^i dx^j \quad (2.9)$$

where $a(t)$ is the scale factor. Using $n^2(t) = 1$, the Friedmann equations on the FLRW background are obtained from the $(0,0)$ and (i,j) components of Einstein equations (2.2)

$$3M_{\text{Pl}}^2 H^2 = -\frac{1}{2}c_2 \dot{\pi}^2 + \frac{3}{M^3} c_3 H \dot{\pi}^3 + \rho_c + \rho_b + \rho_r, \quad (2.10)$$

$$M_{\text{Pl}}^2 (3H^2 + 2\dot{H}) = \frac{1}{2}c_2 \dot{\pi}^2 + \frac{1}{M^3} c_3 \dot{\pi}^2 \ddot{\pi} - \frac{1}{3}\rho_r, \quad (2.11)$$

where $H = \dot{a}/a$ is Hubble expansion rate. Here a dot denote derivative with respect to time.

From Eqs. (2.10) and (2.11), we identify the effective density and pressure of the Galileon field

$$\rho_x = -\frac{1}{2}c_2 \dot{\pi}^2 + \frac{3}{M^3} c_3 H \dot{\pi}^3, \quad (2.12)$$

$$P_x = -\frac{1}{2}c_2 \dot{\pi}^2 - \frac{1}{M^3} c_3 \dot{\pi}^2 \ddot{\pi}. \quad (2.13)$$

In the FLRW space-time Eq.(2.7) reads

$$\dot{\rho}_x + 3H(\rho_x + P_x) = Q, \quad (2.14)$$

$$\dot{\rho}_c + 3H\rho_c = -Q. \quad (2.15)$$

Additionally, the conservation laws for radiation and baryon components on the background read

$$\dot{\rho}_r + 4H\rho_r = 0, \quad \dot{\rho}_b + 3H\rho_b = 0. \quad (2.16)$$

Once a form of the interaction Q is known, the background dynamics is fully determined by the energy conservation equations (2.14) and (2.15) and the Friedmann equations (2.10) and (2.11).

Let us take benefit of the existence of a de Sitter (dS) background characterized by $H = H_{\text{dS}} \equiv cst$, $\dot{\pi} = \dot{\pi}_{\text{dS}} \equiv cst$, and fix the free parameters c_2, c_3 in the Galileon Lagrangian in terms of the interaction function. Writing the dynamical equations in the dS era, and solving the resulting equations we obtain

$$x_{\text{dS}}^2 c_2 = 6, \quad x_{\text{dS}}^3 c_3 = 2 + \frac{Q_{\text{dS}}}{9H_{\text{dS}}^3 M_{\text{Pl}}^3}, \quad (2.17)$$

$$\Omega_{\text{b,dS}} = 0, \quad \Omega_{\text{c,dS}} = -\frac{Q_{\text{dS}}}{9H_{\text{dS}}^3 M_{\text{Pl}}^2}. \quad (2.18)$$

where $x_{\text{dS}} = \frac{\dot{\pi}_{\text{dS}}}{H_{\text{dS}} M_{\text{Pl}}}$ and we normalized M to $M^3 = M_{\text{Pl}} H_{\text{dS}}^2$ [69]. These equations indicate that Q_{dS} must be negative, implying an energy flow from dark energy (DE) to dark matter (DM) during the de Sitter (dS) era. Notably, the only pertinent free parameters are the coupling parameters within the interaction function, and the DM density during the dS era is non-zero, contingent upon the coupling function.

Indeed, deriving the exact form of Q from fundamental principles is elusive, and the existing forms are typically derived phenomenologically or inspired by investigations in scalar-tensor theories [70]. Among the diverse interaction terms explored in literature, we adopt the coupling function described in [68]:

$$Q = H\alpha\rho_x, \quad (2.19)$$

where α is the coupling constant and αH is the rate of transfer of DE to DM.

In this case the Galileon field equation, Eq.(2.14) reads

$$2\ddot{\pi} (8c_3 H\dot{\pi}^2 - c_2 M^3 \dot{\pi}) + 6c_3 \dot{\pi}^3 (\dot{H} - (\alpha - 1)H^2) + (\alpha - 2)c_2 M^3 H\dot{\pi}^2 = 0, \quad (2.20)$$

and Eqs.(2.17) and (2.18) reduce to

$$x_{\text{dS}}^2 c_2 = 6, \quad x_{\text{dS}}^3 c_3 = \frac{\alpha - 6}{\alpha - 3}, \quad \Omega_{\text{b,dS}} = 0, \quad \Omega_{\text{c,dS}} = \frac{\alpha}{\alpha - 3}. \quad (2.21)$$

We proceed to examine the background dynamics employing autonomous dynamical systems. Initially, we simplify the evolution equations (2.10) and (2.11) into more manageable first-order differential equations by introducing new dimensionless dynamical variables. To accomplish this, we adopt the methodology outlined in the non-interacting case in [71], introducing the dimensionless variables r_1 and r_2 :

$$r_1 = \frac{\dot{\pi}_{\text{dS}} H_{\text{dS}}}{\dot{\pi} H}, \quad r_2 = \frac{1}{r_1} \left(\frac{\dot{\pi}}{\dot{\pi}_{\text{dS}}} \right)^4, \quad (2.22)$$

and the definitions

$$\epsilon_H = \frac{\dot{H}}{H^2}, \quad \epsilon_\pi = \frac{\ddot{\pi}}{\dot{\pi} H}. \quad (2.23)$$

Then we easily obtain:

$$\frac{H}{H_{\text{dS}}} = \frac{1}{r_1 (r_1 r_2)^{1/4}}, \quad \frac{\dot{\pi}}{\dot{\pi}_{\text{dS}}} = (r_1 r_2)^{1/4}. \quad (2.24)$$

In the dS phase, where $H = H_{\text{dS}} \equiv \text{cst}$, $\dot{\pi} = \dot{\pi}_{\text{dS}} \equiv \text{cst}$, we get $r_1 = r_2 = 1$.

The dimensionless variables $r_1, r_2, \Omega_b, \Omega_r$ obey the differential equations

$$r_1' = -r_1 (\epsilon_\pi + \epsilon_H), \quad (2.25)$$

$$r_2' = r_2 (5\epsilon_\pi + \epsilon_H), \quad (2.26)$$

$$\Omega_r' = -\Omega_r (4 + 2\epsilon_H), \quad (2.27)$$

$$\Omega_b' = -\Omega_b (3 + 2\epsilon_H), \quad (2.28)$$

where the density parameters are $\Omega_a = \rho_a / (3M_{\text{Pl}}^2 H^2)$, $a = \{r, b, c, x\}$, and the prime denotes derivative with respect to $N = \ln a$. Combining (2.25) and (2.26) we obtain:

$$\epsilon_H = -\frac{5r_1'}{4r_1} - \frac{r_2'}{4r_2}. \quad (2.29)$$

In the non-interacting case ($\alpha = 0$), the standard scenario is restored, consistent with the analysis presented in [71]. Next, we express (2.10), (2.11), and (2.20) in terms of the dimensionless variables and proceed to solve for ϵ_H and ϵ_π :

$$\epsilon_H = (\alpha - 3) \left[\frac{r_1^2 r_2 (r_1 - 1) (\alpha - 6)^2 + 2 (3r_1^3 r_2 - \Omega_r - 3) (\alpha r_1 - \alpha - 3r_1 + 6)}{4(\alpha - 3) (\alpha (r_1 - 1) - 3r_1 + 6) - r_1^2 r_2 (\alpha - 6)^2} \right], \quad (2.30)$$

$$\epsilon_\pi = (\alpha - 3)(\alpha - 6) \left[\frac{3r_1^3 r_2 - \Omega_r - 3 + 2(\alpha - 3)(r_1 - 1)}{4(\alpha - 3)(\alpha(r_1 - 1) - 3r_1 + 6) - r_1^2 r_2 (\alpha - 6)^2} \right]. \quad (2.31)$$

The DE density Ω_x and the DE EoS ω_x are then given in terms of r_1 and r_2 as:

$$\Omega_x = -\frac{r_1^3 r_2 [(\alpha - 3)r_1 + 6 - \alpha]}{\alpha - 3}, \quad (2.32)$$

$$\omega_x = \frac{1 + \left(\frac{\alpha-6}{\alpha-3}\right) \frac{\epsilon_\pi}{3r_1}}{1 - \left(\frac{\alpha-6}{\alpha-3}\right) \frac{1}{r_1}}. \quad (2.33)$$

Let us denote the autonomous system (2.25)-(2.28) generically as:

$$\dot{\vec{x}}_i = f(\vec{x}), \quad \vec{x} = (r_1, r_2, \Omega_r, \Omega_b). \quad (2.34)$$

Firstly, we identify the fixed or critical points of equations (2.34) and investigate their stability throughout cosmic history. The fixed points correspond to the roots of $\dot{\vec{x}}_i = 0$. The stability analysis is conducted using first-order perturbation technique around these fixed points, followed by the formation of the coefficient matrix for the perturbed terms. A fixed point is deemed stable (an attractor) if all eigenvalues of the perturbation matrix are negative, a saddle if the eigenvalues have mixed signs, and unstable if all eigenvalues are positive [72]. We have identified five fixed points, denoted as A , B , C , D , and E . Their properties are summarized in Tab. 1, where $q = -1 - \epsilon_H$ represents the deceleration parameter, and the eigenvalues C_\pm are given by:

$$C_\pm = \frac{3(\alpha - 3)}{2} \left[\frac{3\alpha - 12\alpha + 48 \pm \alpha \sqrt{(3\alpha - 20)(\alpha - 12)}}{\alpha^2 - 24\alpha + 72} \right]. \quad (2.35)$$

Fixed Points	$(r_1, r_2, \Omega_r, \Omega_b)$	Eigenvalues	Stability	q
A	$(0, 0, 1, 0)$	$(1, 1, \frac{5-\alpha}{2}, -\frac{9-5\alpha}{2})$	Unst. $9/5 < \alpha < 5$ Saddle otherwise	1
B	$(0, 0, 0, \Omega_b)$	$(0, 1, \frac{9-2\alpha}{4}, \frac{10\alpha-21}{4})$	Unst. $21/10 < \alpha < 9/2$ Saddle otherwise	1/2
C	$(\frac{\alpha^2-11\alpha+30}{\alpha^2-13\alpha+30}, 0, 1, 0)$	$(8, -\frac{\alpha^2}{10} + \frac{3\alpha}{2} - 5, 1, 1)$	Unst. if $5 < \alpha < 10$ Saddle otherwise	1
D	$(\frac{2\alpha^2-21\alpha+54}{2\alpha^2-24\alpha+54}, 0, 0, \Omega_b)$	$(0, -1, 6, -\frac{\alpha^2}{9} + \frac{3\alpha}{2} - \frac{9}{2})$	Saddle	1
E	$(1, 1, 0, 0)$	$(-4, -3, C_+, C_-)$	Stable if $\alpha < 3$ Unst. otherwise	-1

Table 1: Location, Eigenvalues and Stability of the Critical Points.

The two fixed points A and B represent the eras of radiation and matter domination, respectively, with no contribution from dark energy (DE). They are unstable for $9/5 < \alpha < 5$ and $21/10 < \alpha < 9/2$, respectively, and belong to the small regime [69, 71]. Fixed points C and D also correspond to radiation and matter dominated eras but include contributions from DE. They are unstable for $5 < \alpha < 10$ and saddle, respectively. The last fixed point, E , corresponds to the de Sitter (dS) fixed point. It is stable if $\alpha < 3$ and potentially acts as an attractor for the entire cosmological evolution, regardless of the initial conditions.

We have two viable paths for a valid cosmological evolution. The first/second path begins from the unstable radiation-dominated era, A/C , transitions to the unstable matter-dominated era, B/D , and concludes at the dS point E . It's noteworthy that for $\alpha = 0$, the dynamical analysis conducted above converges with that in [71]. In this case, The point C coincides with A , and the point D coincides with B , and become saddles, while the dS fixed point E remains stable.

2.2 Analysis of the fixed points eras

We'll embark on a detailed analysis of the dynamics within the eras delineated by the fixed points and deduce constraints on the DE-DM coupling.

- *Small regime*

In this regime, the fixed points A and B are characterized by $r_1 \ll 1$ and $r_2 \ll 1$. Under these conditions, the autonomous system of equations simplifies to:

$$r_1' = -\frac{r_1}{4}(2\alpha - \Omega_r - 9), \quad (2.36)$$

$$r_2' = \frac{r_2}{4}(10\alpha + 3\Omega_r - 21), \quad (2.37)$$

$$\Omega_r' = \Omega_r(\Omega_r - 1), \quad (2.38)$$

$$\Omega_b' = \Omega_b\Omega_r. \quad (2.39)$$

These equations integrate to:

$$\Omega_r = \frac{1}{1 + d_4 a}, \quad \Omega_b = \frac{d_1 a}{1 + d_4 a}, \quad (2.40)$$

$$r_1 = \frac{d_3 a^{\frac{5-\alpha}{2}}}{(1 + d_4 a)^{1/4}}, \quad r_2 = \frac{d_2 a^{\frac{5\alpha-9}{2}}}{(1 + d_4 a)^{3/4}}, \quad (2.41)$$

where d_i are constants. The two fixed points in the small regime, A (unstable for $\alpha < 5$) and B (unstable for $\alpha < 9/2$), represent pure radiation-dominated and pure matter-dominated solutions, respectively. In the vicinity of A, we set $d_4 \approx 0$ and obtain:

$$r_1 \approx a^{\frac{5-\alpha}{2}}, \quad r_2 \approx a^{\frac{5\alpha-9}{2}}, \quad H \approx a^{-2}, \quad \pi \approx a^{\frac{\alpha+3}{4}}, \quad (2.42)$$

While for B, we consider d_4 to be very large but with $d_1/d_4 \sim 1$, yielding:

$$r_1 \approx a^{\frac{9-2\alpha}{4}}, \quad r_2 \approx a^{\frac{10\alpha-21}{4}}, \quad H \approx a^{-3/2}, \quad \pi \approx a^{\frac{2\alpha+3}{4}}. \quad (2.43)$$

We observe that the exponents of the scale factor in (2.42) and (2.43) precisely match the eigenvalues of fixed points A and B, respectively. Additionally, for $9/5 < \alpha < 5$, r_2 grows faster than r_1 . We also derive the conventional evolution laws of the Hubble parameter during the radiation and matter domination epochs, regardless of the DE-DM coupling constant. This outcome is anticipated since the interaction term, proportional to ρ_{DE} , only becomes significant at the onset of the DE-dominated epoch.

In the small regime, the DE and the total effective equation of state (EoS) are approximated by:

$$w_x \approx -\frac{1}{12} \left[\frac{2(r_1^2 + 1)\alpha^2 + (2(\Omega_r + 6)r_1 + \Omega_r - 15)\alpha - 6\Omega_r(r_1 + 1) + 18(1 - 3r_1)}{\alpha - 6} \right], \quad (2.44)$$

$$w_{\text{eff}} \approx \frac{\Omega_r}{3}. \quad (2.45)$$

For the radiation dominated fixed point A we have:

$$w_x = \frac{1}{6} - \frac{\alpha}{6}, \quad w_{\text{eff}} = \frac{1}{3}, \quad (2.46)$$

while for the matter dominated fixed point B we have:

$$w_x = \frac{1}{4} - \frac{\alpha}{6}, \quad w_{\text{eff}} = 0. \quad (2.47)$$

In the non-interacting cubic Galileon model ($\alpha = 0$), we approximate the solutions as follows: $r_1 \approx a^{5/2}$, $r_2 \approx a^{-9/2}$, $H \approx a^{-2}$, $w_x = 1/6$ for point A, and $r_1 \approx a^{9/4}$, $r_2 \approx a^{-21/4}$, $H \approx a^{-3/2}$, $w_x = 1/4$ for point B. These behaviors differ from those in ref. [69] where $r_1 \approx a^{5/4}$, $r_2 \approx a^{7/4}$, $H \approx a^{-2}$, and $w_x = 1/4$ in the radiation era, and $r_1 \approx a^{9/4}$, $r_2 \approx a^{3/8}$, $H \approx a^{-93/32}$, and $w_x = 1/8$ in the matter era. The discrepancy originates from numerical factors (1/8 instead of 1/4) in Eqs. (2.36) and (2.37).

• **Fixed Point C**

This point exhibits instability within the interval $5 < \alpha < 10$, corresponding to a pure radiation-dominated solution. In its vicinity, the parameter r_2 becomes small. Consequently, the DE density, DE EoS, and the effective EoS are approximately described by:

$$\Omega_x = 5 \left[\frac{(\alpha - 6)^3 (\alpha - 5)^2}{(\alpha - 3)^3 (\alpha - 10)^3} \right] r_2, \quad (2.48)$$

$$w_x = \frac{\alpha}{3} - \frac{7}{3} - \frac{1}{60} \left[\frac{(\alpha - 6)^3 (\alpha - 5)^2 (\alpha - 7)}{(\alpha - 3)^3 (\alpha - 10)} \right] r_2, \quad (2.49)$$

$$w_{\text{eff}} = \frac{1}{3} + \frac{5}{3} \left[\frac{(\alpha - 6)^3 (\alpha - 5)^2 (\alpha - 7)}{(\alpha - 3)^3 (\alpha - 10)^3} \right] r_2. \quad (2.50)$$

At the fixed point, $r_2 = 0$, we are left with the results

$$\Omega_x = 0, \quad w_x = -\frac{7}{3} + \frac{\alpha}{3}, \quad w_{\text{eff}} = \frac{1}{3}. \quad (2.51)$$

• **Fixed Point D**

This fixed point is saddle and corresponds to a pure matter-dominated solution. In this phase, we can expand the DE density, the DE EoS, and the effective EoS around $r_2 \ll 1$ to obtain:

$$\Omega_x = \frac{9}{8} \left[\frac{(2\alpha - 9)^2 (\alpha - 6)^3}{(\alpha - 3)^3 (\alpha - 9)^3} \right] r_2, \quad (2.52)$$

$$w_x = \frac{\alpha}{3} - 2 - \frac{1}{216} \left[\frac{(2\alpha - 9)^2 (\alpha - 6)^4}{(\alpha - 3)^3 (\alpha - 9)} \right] r_2, \quad (2.53)$$

$$w_{\text{eff}} = \frac{3}{8} \left[\frac{(2\alpha - 9)^2 (\alpha - 6)^3}{(\alpha - 3)^3 (\alpha - 9)^3} \right] r_2. \quad (2.54)$$

At exactly the fixed point, $r_2 = 0$, we have

$$\Omega_x = 0, \quad w_x = -2 + \frac{\alpha}{3}, \quad w_{\text{eff}} = 0. \quad (2.55)$$

- *dS Fixed Point*

The dS fixed point characterized by $r_1 = 1$, $r_2 = 1$ is stable for $\alpha < 3$. At this point we have

$$\Omega_{c,\text{dS}} = \frac{\alpha}{\alpha - 3}, \quad \Omega_{x,\text{ds}} = \frac{3}{3 - \alpha}, \quad w_{x,\text{ds}} = -1 + \frac{\alpha}{3}, \quad w_{\text{eff,dS}} = -1. \quad (2.56)$$

We detect deviations from the standard Λ CDM model when $\alpha \neq 0$. Specifically, during the de Sitter (dS) era, DE continues to dominate, albeit with a minor contribution from DM. This arises from the gradual decay of the DE fields into DM, resulting in a constant fraction $\Omega_{c,\text{dS}}$ throughout the dS era. Additionally, we observe that the EoS w_x deviates slightly from -1 . By combining constraints on the solutions and ensuring the positivity of the DM density during the dS era, we infer that $\alpha < 0$.

- *Tracker Solution*

Assuming a small coupling α in the dark sector, we note from Table (1) that the coordinate r_1 for the fixed points C and D is of order unity. Following the approach outlined in [71], we approximate the dynamics of the model by setting $r_1 = 1$ in the dynamical equations and solving for r_2 , Ω_r , and Ω_b . In this scenario, the autonomous system of equations (2.26)-(2.28) can be expressed as:

$$\frac{r_2'}{r_2} = (\alpha - 3) \left[\frac{(5\alpha - 24)(\Omega_r - 3r_2 + 3)}{\alpha^2 r_2 - 12(\alpha - 3)(r_2 + 1)} \right], \quad (2.57)$$

$$\frac{\Omega_r'}{\Omega_r} = -4 \left[\frac{\alpha^2 r_2 + 3(\alpha - 3)(\Omega_r - 7r_2 - 1)}{\alpha^2 r_2 - 12(\alpha - 3)(r_2 + 1)} \right], \quad (2.58)$$

$$\frac{\Omega_b'}{\Omega_b} = -3 \left[\frac{\alpha^2 r_2 + 4(\alpha - 3)(\Omega_r - 6r_2)}{\alpha^2 r_2 - 12(\alpha - 3)(r_2 + 1)} \right]. \quad (2.59)$$

Combining these equations we obtain

$$\frac{r_2'}{r_2} - \gamma \left(\frac{\Omega_r'}{\Omega_r} - 4 \right) = 0, \quad \frac{r_2'}{r_2} - \gamma \left(\frac{\Omega_b'}{\Omega_b} + 3 \right) = 0, \quad \gamma = 2 - \frac{5\alpha}{12}. \quad (2.60)$$

The solution of Eqs.(2.60) are

$$r_2(a) = r_2(0) a^{4\gamma} \left(\frac{\Omega_r(a)}{\Omega_r(0)} \right)^\gamma, \quad r_2(a) = r_2(0) a^{3\gamma} \left(\frac{\Omega_b(a)}{\Omega_b(0)} \right)^\gamma. \quad (2.61)$$

Using (2.29), we obtain:

$$H(a) = H(0) a^{-\gamma} \left(\frac{\Omega_r(a)}{\Omega_r(0)} \right)^{-\gamma/4}. \quad (2.62)$$

The DE density, the DE EoS, and the effective EoS parameters along the tracker are now given by

$$\Omega_x = \frac{3r_2}{3 - \alpha}, \quad (2.63)$$

$$w_x = \left(\frac{\alpha - 3}{9} \right) \left[\frac{(\Omega_r + 3)\alpha^2 - 12(\alpha - 3)(\Omega_r + 6)}{[r_2\alpha^2 - 12(\alpha - 3)(r_2 + 1)]} \right],$$

$$w_{\text{eff}} = - \left[\frac{r_2 \alpha^2 + 4(\alpha - 3)(\Omega_r - 6r_2)}{r_2 \alpha^2 - 12(\alpha - 3)(1 + r_2)} \right]. \quad (2.64)$$

We observe that the DE density reach the solution in the dS era for $r_2 = 1$. When $\alpha = 0$, we reproduce exactly the relations of [71]

$$\Omega_x = r_2, \quad w_x = -\frac{\Omega_r + 6}{3(r_2 + 1)}, \quad w_{\text{eff}} = \frac{(\Omega_r - 6r_2)}{3(1 + r_2)}. \quad (2.65)$$

Although we can express all the relevant quantities along the tracker in terms of Ω_r , obtaining an algebraic equation for Ω_r and solving it as done in [71] is not feasible. Therefore, we substitute (2.61) into (2.58) and (2.59) and numerically integrate the resulting equations. Finally, assuming that $\Omega_{c\text{dS}} \geq 0$, we derive the constraint $\alpha \leq 0$.

3 ICG on the perturbed flat space-time

The investigation of the growth rate of cosmological density perturbations has emerged as a potent tool for distinguishing between cosmological models based on modified theories of gravity and DE based models. While all models may perfectly mimic the Λ CDM evolution at the background level, they inherently influence structure formation. An important aspect in this regard is the evolution of the linear matter density contrast $\delta_m \equiv \delta\rho_m/\rho_m$, which satisfies the equation:

$$\ddot{\delta}_m + 2H\dot{\delta}_m - 4\pi G_{\text{eff}}\rho_m \approx 0. \quad (3.1)$$

Here, G_{eff} is the effective gravitational constant, function of the scale factor and the cosmological scale. The matter density contrast is linked to the observed quantity $f(a)\sigma_8(a)$, where $f(a) = d\ln\delta(a)/d\ln(a)$ and $\sigma_8(a) = \sigma_8\delta_m(a)/\delta_m(1)$ represents the root mean square fluctuations of the linear density field within a radius of $8h^{-1}\text{Mpc}$, with σ_8 being its present value.

Scalar perturbations on a flat FLRW spacetime in the conformal Newtonian gauge are described by the following metric:

$$ds^2 = -a^2(\eta) [(1 + 2\psi)d\eta^2 - \delta_{ij}(1 - 2\theta)dx^i dx^j]. \quad (3.2)$$

Here, ψ and θ describe scalar perturbations, with ψ being the gravitational potential.

In cosmological perturbations theory, each quantity, denoted by χ , is expanded up to the desired order with a homogeneous background $\bar{\chi}$ and a small part $\delta\chi = \sum_{n=1}^{\infty} \frac{\chi_n}{n!}$, where n denotes the perturbation order. Here, we specifically focus on linear perturbation theory, i.e., where $n = 1$.

3.1 Perturbed energy momentum tensor

We are concerned with matter and dark energy dominated eras where the anisotropic stress can be neglected. In such cases, the energy-momentum tensor of a fluid A is given by:

$$T_{\mu\nu}^{(A)} = T_{\mu\nu}^{(A)} = (\rho_A + P_A) u_\mu u_\nu + P_A g_{\mu\nu}, \quad (3.3)$$

$$\rho_A = \bar{\rho}_A + \delta\rho_A, \quad P_A = \bar{P}_A + \delta P_A. \quad (3.4)$$

Here $\bar{\rho}_A$, \bar{P}_A are energy density and pressure on the background, u_A^μ is the A -fluid four velocity given by:

$$u_A^\mu = a^{-1} (1 - \psi, v_A^i), \quad v_A^i = \partial^i u_A, \quad (3.5)$$

and u_A is the peculiar velocity potential.

The total energy-momentum tensor is the sum of the energy-momentum tensor of the individual fluids:

$$T_{\mu\nu} = \sum_A T_{\mu\nu}^{(A)} = (\rho + P) u_\mu u_\nu + P g_{\mu\nu}, \quad (3.6)$$

where

$$\rho = \sum_A \rho_A, \quad P = \sum_A P_A, \quad u^\mu = a^{-1} (1 - \psi, \partial^i u), \quad (3.7)$$

and the total velocity potential u is defined by:

$$(\rho + p) u = \sum (\rho_A + p_A) u_A. \quad (3.8)$$

The energy-momentum tensor of each component is not conserved, and its divergence introduces a local energy-momentum transfer tensor Q_A^μ :

$$\nabla_\nu T_A^{\mu\nu} = Q_A^\mu. \quad (3.9)$$

Here, Q_A^μ is referred to as the covariant interaction function, often expressed as:

$$Q_A^\mu = Q_A u^\mu + f_A^\mu, \quad (3.10)$$

where the functions Q_A and f_A^μ denote the energy density transfer rate and the momentum density transfer rate to the A -component as observed in the center of mass frame:

$$Q_A = \bar{Q}_A + \delta Q_A, \quad f_A^\mu = a^{-1} (f_A^0, \partial^i f_A), \quad u_\mu f_A^\mu = 0, \quad (3.11)$$

where, f_A represents a momentum transfer potential. From the conservation law of the total energy-momentum tensor $\nabla_\nu T^{\mu\nu} = 0$, the coupling function Q_A^μ is constrained by:

$$\sum_A Q_A = \sum_A \delta Q_A = \sum_A f_A = 0. \quad (3.12)$$

Given the orthogonality relation between f_A^μ and u_μ , it follows that $f_A^0 = 0$, and hence:

$$f_A^\mu = a^{-1} (0, \partial^i f_A). \quad (3.13)$$

By combining (3.11) and (3.13) with (3.5), we arrive at:

$$Q_A^0 = a^{-1} [\bar{Q}_A (1 - \psi) + \delta Q_A], \quad (3.14)$$

$$Q_A^i = a^{-1} \partial^i (\bar{Q}_A u + f_A). \quad (3.15)$$

At zero order we have $Q_A^\mu = a^{-1} (\bar{Q}_A, \vec{0})$. This indicates the absence of momentum transfer on the background.

For coupled DM and DE fluids, $A = x, c$, we have:

$$\nabla_\mu T_{(x)}^{\mu\nu} = Q_{(x)}^\nu, \quad \nabla_\mu T_{(c)}^{\mu\nu} = Q_{(c)}^\nu, \quad (3.16)$$

where $Q_{(c)}^\nu = -Q_{(x)}^\nu$. On the background Eq.(3.16) becomes:

$$\bar{\rho}'_c + 3\mathcal{H}\bar{\rho}_c = -a\bar{Q}_x, \quad (3.17)$$

$$\bar{\rho}'_x + 3\mathcal{H}(\bar{\rho}_x + \bar{P}_x) = a\bar{Q}_x, \quad (3.18)$$

where $\mathcal{H} = aH$ is Hubble parameter in terms of conformal time. Let us define the density contrast $\delta_A = \delta\rho_A/\rho_A$ of the fluid A, with $\delta T_{0A}^0 = -\delta\rho_A$, $\delta T_{iA}^0 = (\bar{\rho}_A + \bar{P}_A)v_{iA} = -\delta T_{0A}^i$ and $\delta T_{jA}^i = \delta P_A \delta_j^i$. Then, the perturbed energy and momentum balance equations of DM are obtained from Eq.(3.16) as follows:

$$\delta'_c + \nabla^2 u_c - 3\theta' = \frac{a}{\bar{\rho}_c} (\bar{Q}_c \psi + \delta Q_c - \bar{Q}_c \delta_c) \quad (3.19)$$

$$(\bar{\rho}_c u_c)' + \psi \bar{\rho}_c + 4\mathcal{H} \bar{\rho}_c u_c = a\bar{Q}_c u + a f_c. \quad (3.20)$$

Substituting Eq.(3.17) into Eq.(3.20), we arrive at:

$$u'_c + \mathcal{H} u_c + \psi = \frac{a}{\bar{\rho}_c} (\bar{Q}_c (u - u_c) + f_c). \quad (3.21)$$

Now, turning our attention to the DE component, let Π represent the perturbed Galileon field, $\Pi(\eta, x^i) = \pi(\eta) + \delta\pi(\eta, x^i)$, and $T_{\alpha\beta}^{(x)} = \bar{T}_{\alpha\beta}^{(x)} + \delta T_{\alpha\beta}^{(x)}$, its energy momentum tensor, where $\bar{T}_{00}^{(x)} = \rho_x$, $\bar{T}_{0i}^{(x)} = 0 = T_{i0}^{(x)}$ and $\bar{T}_{ij}^{(x)} = P_x g_{ij}$ are given by Eqs.(2.12-2.13). The perturbed part of $T_{\alpha\beta}^{(x)}$ read as:

$$\delta T_{00}^{(x)} = -\pi' \left[\left(c_2 - \frac{9c_3}{a^2 M^3} \mathcal{H} \pi' \right) \delta\pi' + \frac{c_3}{a^2 M^3} (\pi' \nabla^2 \delta\pi + 6\mathcal{H} \pi' \psi + \pi'^2 \theta') \right], \quad (3.22)$$

$$\delta T_{0i}^{(x)} = -\pi' \partial_i \left[\frac{c_3}{a^2 M^3} \pi' \delta\pi' + \left(c_2 - \frac{3c_3}{a^2 M^3} \mathcal{H} \pi' \right) \delta\pi - \frac{c_3}{a^2 M^3} \pi'^2 \psi \right], \quad (3.23)$$

$$\begin{aligned} \delta T_{ij}^{(x)} = & \pi' \left[-\frac{c_3}{a^2 M^3} \pi' \delta\pi'' + \frac{c_3}{a^2 M^3} \pi'^2 \psi' + \left(-c_2 + \frac{c_3}{a^2 M^3} (3\mathcal{H} \pi' - 2\pi'') \right) \delta\pi' \right. \\ & \left. + \left(c_2 + \frac{4c_3}{a^2 M^3} (\pi'' - \mathcal{H} \pi') \right) \pi' \psi + \left(c_2 + \frac{2c_3}{a^2 M^3} (\pi'' - \mathcal{H} \pi') \right) \pi' \theta \right] \delta_{ij}. \end{aligned} \quad (3.24)$$

The perturbed equation of motion of the Galileon field follows from (3.16) for $\nu = 0$:

$$\begin{aligned} & \left(c_2 - \frac{6c_3}{a^2 M^3} \mathcal{H} \pi' \right) \pi' (\delta\pi)'' + \left[c_2 (\pi'' + 4\mathcal{H} \pi') - \frac{3c_3}{a^2 M^3} (4\mathcal{H} \pi'' + 3\mathcal{H}' \pi') \right] \pi' (\delta\pi)' + \\ & \left[-c_2 + \frac{2c_3}{a^2 M^3} (\pi'' + \mathcal{H} \pi') \right] \pi' \nabla^2 (\delta\pi) + \left(-c_2 + \frac{9c_3}{a^2 M^3} \mathcal{H} \pi' \right) \pi'^2 \psi' + \\ & \left[c_2 (-2\pi'' - 4\mathcal{H} \pi') + \frac{12c_3}{a^2 M^3} (2\mathcal{H} \pi' \pi'' + \mathcal{H}' \pi'^2) \right] \pi' \psi + \frac{c_3}{a^2 M^3} \pi'^3 \nabla^2 \psi + \\ & \frac{3c_3}{a^2 M^3} \pi'^3 \theta'' + 3 \left[-c_2 + \frac{c_3}{a^2 M^3} (2\pi'' + 3\mathcal{H} \pi') \right] \pi'^2 \theta' \\ = & -a^3 \left(\bar{Q}_{(x)} \psi + Q_{(x)}^{(1)} \right). \end{aligned} \quad (3.25)$$

The component $\nu = i$ of (3.16) leads to:

$$\left[c_2 (\pi'' + 2\mathcal{H} \pi') + \frac{c_3}{a^2 M^3} (-3\mathcal{H}' \pi'^2 - 3\mathcal{H}^2 \pi'^2 - 6\mathcal{H} \pi' \pi'' + 3\mathcal{H}^2 \pi'') \right] \delta\pi = a^3 \left(\bar{Q}_x u + f_x^{(1)} \right). \quad (3.26)$$

Utilizing the Galileon field equation on the background:

$$c_2 (\pi'' + 2\mathcal{H} \pi') \pi' - \frac{c_3}{a^2 M^3} (6\mathcal{H} \pi'' + 3\mathcal{H}' \pi') \pi'^2 = -a^3 \bar{Q}_{(x)}, \quad (3.27)$$

the equations (3.25-3.26) simplify to:

$$\begin{aligned}
& \left(c_2 - \frac{6c_3}{a^2 M^3} \mathcal{H} \pi' \right) \pi'^2 (\delta\pi)'' + \left[2c_2 \mathcal{H} - \frac{3c_3}{a^2 M^3} (2\mathcal{H} \pi'' + 2\mathcal{H}' \pi') \right] \pi'^2 (\delta\pi)' + \\
& \left[-c_2 + \frac{2c_3}{a^2 M^3} (\pi'' + \mathcal{H} \pi') \right] \pi'^2 \nabla^2 (\delta\pi) + \left(-c_2 + \frac{9c_3}{a^2 M^3} \mathcal{H} \pi' \right) \pi'^3 \psi' + \\
& \left[c_2 (-2\pi'' - 4\mathcal{H} \pi') + \frac{12c_3}{a^2 M^3} (2\mathcal{H} \pi' \pi'' + \mathcal{H}' \pi'^2) \right] \pi'^2 \psi + \frac{c_3}{a^2 M^3} \pi'^4 \nabla^2 \psi + \\
& \frac{3c_3}{a^2 M^3} \pi'^4 \theta'' - 3 \left[c_2 - \frac{c_3}{a^2 M^3} (2\pi'' + 3\mathcal{H} \pi') \right] \pi'^3 \theta' \\
& = -a^3 \left(\bar{Q}_{(x)} \psi + Q_{(x)}^{(1)} \right) \pi' - \bar{Q}_{(x)} (\delta\pi)', \tag{3.28}
\end{aligned}$$

and

$$\left(\frac{3c_3 \mathcal{H}^2}{a^2 M^3} (-\pi'^2 + \pi'') \pi' + a^3 \bar{Q}_{(x)} \right) \delta\pi = a^3 \left(\bar{Q}_x u + f_x^{(1)} \right) \pi'. \tag{3.29}$$

In the absence of DE-DM coupling, we recover the equations in [73]. Finally, the equations of the density and velocity perturbations for the baryon fluid remain the usual ones in the absence of DM-DE interaction:

$$\delta_b' + \nabla^2 u_b - 3\theta' = 0, \tag{3.30}$$

$$u_b' + \mathcal{H} u_b + \psi = 0. \tag{3.31}$$

3.2 Perturbed Einstein equations

To linear order in the perturbation, the (0, 0) component of Einstein equations reads as:

$$\begin{aligned}
& 2M_{\text{Pl}}^2 \nabla^2 \theta - \left(2a^2 \bar{\rho}_m - \frac{6c_3}{a^2 M^3} \mathcal{H} \pi'^3 \right) \psi + \left(\frac{3c_3}{a^2 M^3} \pi'^3 - 6M_{\text{Pl}}^2 \mathcal{H} \right) \theta' \\
& = a^2 \delta\rho_m - \frac{c_3}{a^2 M^3} \pi'^2 \nabla^2 \delta\pi - \left(c_2 \pi' - \frac{9c_3}{a^2 M^3} \mathcal{H} \pi'^2 \right) \delta\pi', \tag{3.32}
\end{aligned}$$

where $\bar{\rho}_m = \bar{\rho}_c + \bar{\rho}_b$, $\delta\rho_m = \bar{\rho}_m \delta_m = \bar{\rho}_c \delta_c + \bar{\rho}_b \delta_b$, $\delta_c = \delta\rho_c / \bar{\rho}_c$ and $\delta_b = \delta\rho_b / \bar{\rho}_b$. Substituting Friedmann's equation (2.10) into (3.32), we obtain:

$$\begin{aligned}
& 2M_{\text{Pl}}^2 \nabla^2 \theta - \left(6M_{\text{Pl}}^2 \mathcal{H}^2 + c_2 \pi'^2 - \frac{12c_3}{a^2 M^3} \mathcal{H} \pi'^3 \right) \psi + \left(-6M_{\text{Pl}}^2 \mathcal{H} + \frac{3c_3}{a^2 M^3} \pi'^3 \right) \theta' \\
& = a^2 \delta\rho_m - \frac{c_3}{a^2 M^3} \pi'^2 \nabla^2 \delta\pi - \left(c_2 \pi' - \frac{9c_3}{a^2 M^3} \mathcal{H} \pi'^2 \right) \delta\pi'. \tag{3.33}
\end{aligned}$$

The (0, i) component of Einstein equations is:

$$\partial_i \left[2M_{\text{Pl}}^2 \theta' + \left(2M_{\text{Pl}}^2 \mathcal{H}^2 - \frac{c_3}{a^2 M^3} \pi'^3 \right) \psi + \left(c_2 \pi' - \frac{3c_3}{a^2 M^3} \mathcal{H} \pi'^2 \right) \delta\pi + \frac{c_3}{a^2 M^3} \pi'^2 \delta\pi' \right] = -a^2 \bar{\rho}_m v_i, \tag{3.34}$$

and the (i, j) components leads to:

$$\begin{aligned}
& M_{\text{Pl}}^2 \partial^i \partial_j (\theta - \psi) + [2M_{\text{Pl}}^2 \theta'' + 4M_{\text{Pl}}^2 \mathcal{H} \theta' \\
& + \left(2M_{\text{Pl}}^2 \mathcal{H}^2 + 4M_{\text{Pl}}^2 \mathcal{H}' - c_2 \pi'^2 + \frac{4c_3}{a^2 M^3} \pi'^2 (\mathcal{H} \pi' - \pi'') \right) \psi + \left(2M_{\text{Pl}}^2 \mathcal{H} - \frac{c_3}{a^2 M^3} \pi'^3 \right) \psi'
\end{aligned}$$

$$+ M_{\text{Pl}}^2 \nabla^2 (\psi - \theta) + \left(c_2 \pi' + \frac{c_3}{a^2 M^3} \pi' (2\pi'' - 3\mathcal{H}\pi') \right) \delta\pi' + \frac{c_3}{a^2 M^3} \pi'^2 \delta\pi'' \Big] \delta_j^i = 0. \quad (3.35)$$

As usual we separate this equation into trace and traceless parts as:

$$\begin{aligned} & 2M_{\text{Pl}}^2 \theta'' + 4M_{\text{Pl}}^2 \mathcal{H} \theta' + \left(2M_{\text{Pl}}^2 \mathcal{H}^2 + 4M_{\text{Pl}}^2 \mathcal{H}' - c_2 \pi'^2 + \frac{4c_3}{a^2 M^3} \pi'^2 (\mathcal{H}\pi' - \pi'') \right) \psi' \\ & + \left(2M_{\text{Pl}}^2 \mathcal{H} - \frac{c_3}{a^2 M^3} \pi'^3 \right) \psi + \frac{2}{3} M_{\text{Pl}}^2 \nabla^2 (\psi - \theta) \\ & = - \left(c_2 \pi' + \frac{c_3}{a^2 M^3} \pi' (2\pi'' - 3\mathcal{H}\pi') \right) \delta\pi' - \frac{c_3}{a^2 M^3} \pi'^2 \delta\pi'', \end{aligned} \quad (3.36)$$

$$\left(\partial^i \partial_j - \frac{1}{3} \delta_j^i \nabla^2 \right) (\theta - \psi) = 0. \quad (3.37)$$

The later equation gives $\theta = \psi$, because of the absence of anisotropic stress.

3.3 Quasi static approximation

It is convenient to work in Fourier space, where the scalar modes are expanded as:

$$\Phi \sim \int \Phi_k \exp(i\vec{k} \cdot \vec{x}) d^3k. \quad (3.38)$$

Since matter perturbations evolve on spatial scales much smaller than of the Hubble horizon ($k \gg aH$), we use the so called quasi-static approximation on sub-horizon scales (QSA) where $|\Phi''| \lesssim \mathcal{H} |\Phi'| \ll k^2 |\Phi|$. Then Eqs.(3.19), (3.28) and (3.33) simplify and become:

$$\delta_c' - k^2 u_c - 3\theta' = \frac{a}{\bar{\rho}_c} (\bar{Q}_c \psi + \delta Q_c - \bar{Q}_c \delta_c), \quad (3.39)$$

$$k^2 \theta = \frac{-a^2}{2M_{\text{Pl}}^2} (\bar{\rho}_b \delta_b + \bar{\rho}_c \delta_c) - \frac{c_3}{2a^2 M_{\text{Pl}}^2 M^3} \pi'^2 k^2 (\delta\pi), \quad (3.40)$$

$$\left(c_2 - \frac{2c_3}{a^2 M^3} (\pi'' + \mathcal{H}\pi') \right) \pi'^2 k^2 (\delta\pi) - \frac{c_3}{a^2 M^3} \pi'^4 k^2 \theta = -a^3 \delta Q_{(x)} \pi'. \quad (3.41)$$

Solving Eqs.(3.40-3.41) we obtain:

$$\delta\pi = - \frac{(\bar{\rho}_b \delta_b + \bar{\rho}_c \delta_c) c_3 \pi'^4 + 2M_{\text{Pl}}^2 M^3 a^3 \delta Q_{(x)} \pi'}{2M_{\text{Pl}}^2 M^3 k^2 \left[\left(c_2 - \frac{2c_3}{a^2 M^3} (\pi'' + \mathcal{H}\pi') \right) \pi'^2 + \frac{c_3^2}{2a^4 M_{\text{Pl}}^2 M^6} \pi'^6 \right]}. \quad (3.42)$$

Differentiating Eq.(3.39) with respect to the conformal time, and using (3.21), (3.39) and (3.40), we get:

$$\begin{aligned} \delta_c'' + \mathcal{H} \delta_c' &= \frac{a^2}{2M_{\text{Pl}}^2} (\bar{\rho}_b \delta_b + \bar{\rho}_c \delta_c) + \frac{c_3}{2a^2 M_{\text{Pl}}^2 M^3} \pi'^2 k^2 (\delta\pi) + \frac{\mathcal{H}a}{\bar{\rho}_c} (\delta Q_c - \bar{Q}_c \delta_c) + \\ & \left[\frac{a}{\bar{\rho}_c} (\delta Q_c - \bar{Q}_c \delta_c) \right]' + \frac{a}{\bar{\rho}_c} k^2 [\bar{Q}_c (u - u_c) + f_c]. \end{aligned} \quad (3.43)$$

Following same steps we obtain the evolution of the baryon matter perturbation

$$\delta_b'' + \mathcal{H} \delta_b' = \frac{a^2}{2M_{\text{Pl}}^2} (\bar{\rho}_b \delta_b + \bar{\rho}_c \delta_c) + c_3 \frac{\pi'^2 k^2}{2a^2 M_{\text{Pl}}^2 M^3} \delta\pi. \quad (3.44)$$

A notable observation from this outcome is the impact exerted by the coupling between dark energy (DE) and dark matter (DM) on the baryon density perturbation.

3.4 Covariant interaction term

As already discussed above, the simplest physical choice for the DE-DM interaction is to assume that there is no momentum transfer in the rest frame of neither DM nor DE [68]. Then we choose

$$Q_c^\mu = Q_c u_c^\mu, \quad (3.45)$$

such that Eqs.(3.14-3.15) read as

$$Q_c^0 = a^{-1} (\bar{Q}_c (1 - \psi) + \delta Q_c), \quad (3.46)$$

$$Q_c^i = a^{-1} \partial^i (\bar{Q}_c u_c^{(1)}) , \quad (3.47)$$

and

$$f_c = Q_c (u_c - u) = -f_x. \quad (3.48)$$

The preceding treatment of perturbations is completely general. Let us specify the form of the energy-momentum transfer rate as [68]:

$$Q_c = -Q_x = -\alpha \frac{\mathcal{H}}{a} \rho_x. \quad (3.49)$$

Substituting Eqs. (3.49) and (3.22) in (3.42) we obtain

$$\delta\pi = -\frac{(\bar{\rho}_b \delta_b + \bar{\rho}_c \delta_c) c_3 \pi'^4}{2M_{\text{Pl}}^2 M^3 k^2 \left[(c_2 - \frac{2c_3}{a^2 M^3} (\pi'' + \mathcal{H}\pi')) \pi'^2 + \frac{\alpha c_3}{M^3} \mathcal{H} \pi'^3 + \frac{c_3^2}{2a^4 M_{\text{Pl}}^2 M^6} \pi'^6 \right]}. \quad (3.50)$$

Inserting (3.50) in (3.43) we obtain

$$\delta_c'' + (1 - \alpha\gamma) \mathcal{H} \delta_c' = 4\pi G a^2 (\bar{\rho}_b \delta_b + \bar{\rho}_c \delta_c) \left(1 - \frac{c_3^2 \pi'^4}{2c_2 a^4 M_{\text{Pl}}^2 M^6 \lambda} \right) + \xi \bar{\rho}_c \delta_c, \quad (3.51)$$

$$\delta_b'' + \mathcal{H} \delta_b' = 4\pi G a^2 (\bar{\rho}_b \delta_b + \bar{\rho}_c \delta_c) \left(1 - \frac{c_3^2 \pi'^4}{2c_2 a^4 M_{\text{Pl}}^2 M^6 \lambda} \right), \quad (3.52)$$

where

$$\lambda = 1 - \frac{2c_3}{c_2 a^2 M^3} (\pi'' + \mathcal{H}\pi') + \frac{c_3^2}{2c_2 a^4 M_{\text{Pl}}^2 M^6} \pi'^4 + \frac{\alpha c_3}{c_2 M^3} \mathcal{H} \pi', \quad (3.53)$$

and

$$\xi = \frac{\alpha}{\bar{\rho}_c} (\mathcal{H}^2 \gamma + \mathcal{H}' \gamma + \mathcal{H} \gamma'), \quad \gamma = \frac{\bar{\rho}_x}{\bar{\rho}_c}. \quad (3.54)$$

Clearly, the growth rate of matter in Λ CDM is recovered for $c_3 = 0$ and $\alpha = 0$.

For numerical purpose it is useful to work in terms of the time $N = \ln(a)$ and the dimensionless variables of Sec.(2.1). Adopting the notation $\frac{df}{dN} = f'$, straightforward calculations lead to the relations:

$$\delta_c'' + (2 - \alpha\gamma + \epsilon_H) \delta_c' = \frac{3}{2} (G_{cc} \bar{\Omega}_{cc} \delta_c + G_{cb} \bar{\Omega}_b \delta_b), \quad (3.55)$$

$$\delta_b'' + (2 + \epsilon_H) \delta_b' = \frac{3}{2} (G_{bb} \bar{\Omega}_b \delta_b + G_{bc} \bar{\Omega}_c \delta_c), \quad (3.56)$$

where the effective gravitational constants are given by:

$$G_{bb} = 1 - \left(\frac{\alpha - 6}{\alpha - 3} \right)^2 \frac{r_1 r_2}{12\lambda}, \quad G_{cc} = G_{bb} + \xi, \quad G_{cb} = G_{bc} = G_{bb}, \quad (3.57)$$

$$\lambda = 1 - \frac{(\alpha - 6)}{3(\alpha - 3)r_1} (\epsilon_\pi + 2) + \left(\frac{\alpha - 6}{\alpha - 3} \right)^2 \frac{r_1 r_2}{12} + \frac{\alpha(\alpha - 6)}{(\alpha - 3)} \frac{1}{6r_1}, \quad (3.58)$$

$$\xi = \frac{2\alpha\gamma}{3\Omega_c} (2 + \epsilon_H + \alpha(1 + \gamma) - 3\omega_x), \quad (3.59)$$

and ϵ_H , ϵ_π are given by Eqs.(2.30) and (2.31).

As a result of unequal couplings for DM and baryons, we expect the existence of a bias between baryons and DM. We study this in the DM dominated scenario, $|\Omega_c \delta_c| \gg |\Omega_b \delta_b|$, and define a constant bias b , by $\delta_b = b \delta_c$. We can easily determine the bias by writing Eqs. (3.55) and (3.56) in terms of the DM growth parameter $f_c = d \ln(\delta_c) / dN$. Indeed, we easily find

$$b = \frac{2f_c(2 - \alpha\gamma + \epsilon_H + \delta_c) + 3(G_{bc} - G_{cc})\Omega_c}{2f_c(2 + \epsilon_H + \delta_c)}. \quad (3.60)$$

In the limit $\alpha \rightarrow 0$, we have $G_{cc} \rightarrow G_{bc}$, and then $b = 1$.

4 Methodology and data

In this section, we establish observational constraints on the cubic covariant Galileon field coupled to dark matter through the application of a Markov Chain Monte Carlo (MCMC) integration using the Metropolis-Hastings algorithm. We use the recent compilation of redshift space distortion (RSD) datasets, with a specific emphasis on the lowermost 21 data points [74, 75] and the model-independent observational Hubble dataset (OHD) [76] listed in the Table in appendix A. We also utilize combined data from Cosmic Microwave Background (CMB) observations and Baryon Acoustic Oscillations (BAO) based on the Planck 2015 distance prior and a set of BAO measurements [77]. Additionally, we include the efficient catalog of six measurements of $E^{-1}(z) = (H(z)/H_0)^{-1}$, whose efficacy was validated for spatially flat cosmologies [78]. These measurements were obtained from a compressed catalog comprising 1052 Type Ia supernovae (SN), supplemented by the MCT set containing 15 SN at redshifts $z > 1$. The resulting combined likelihood function is formulated as:

$$\mathcal{L}(\mathcal{P}) = \mathcal{L}_{\text{BAO/CMB}} \times \mathcal{L}_{\text{RSD}} \times \mathcal{L}_{\text{OHD}} \times \mathcal{L}_{\text{SN}}, \quad (4.1)$$

where \mathcal{P} is the vector of model parameters over which the MCMC integration is performed.

We perform our analysis for the full exact model labeled ICG and the model obtained through the tracker solution labeled TICG, obtained from the ICG by setting $r_1 = 1$ in the dynamical equations. For the ICG model the parameter vector is given by $\mathcal{P} = (\alpha, r_{1i}, r_{2i}, h, \sigma_8)$, while in the TICG model it is $\mathcal{P} = (\alpha, r_{2i}, h, \sigma_8)$, where r_{1i} and r_{2i} are the starting values deep in the radiation epoch. The ICG model has one more parameter than the TICG model and is expected to be more penalized by Bayesian selection. All these free parameters are explored within the range of the conservative flat priors listed in Table I. Without using any fiducial cosmology to correct the $f\sigma_8$ measurements, we confront our

findings at 68%, 95% confidence limits (CL) with the Λ CDM model. All the constraints presented below are derived using `getdist`¹ [79].

Parameter	ICG	TICG	Λ CDM
α	$[-1, 0]$	$[-1, 0]$	–
$r_1^{(0)}$	$[0, 1] \times 10^{-12}$	–	–
$r_2^{(0)}$	$[0, 3] \times 10^{-17}$	$[0, 2] \times 10^{-60}$	–
$\Omega_m^{(0)}$	–	–	$[0.1, 0.4]$
h	$[0.6, 0.9]$	$[0.6, 0.9]$	$[0.6, 0.9]$
σ_8	$[0.5, 1.5]$	$[0.5, 1.5]$	$[0.5, 1.5]$

Table 2: Flat priors on the cosmological parameters.

In addition, we evaluate the goodness of fit using the corrected frequentist Akaike Information Criterion (AIC) [80] defined by:

$$\text{AIC}_c = \text{AIC} + \frac{2k(k+1)}{n-k+1}, \quad (4.2)$$

where AIC is the standard criterion, given by:

$$\text{AIC} = -2 \ln \mathcal{L}_{\max} + 2k, \quad (4.3)$$

where k is the number of estimated parameters in the model, and n the number of data points. The AIC penalizes model complexity by adding twice the number of free parameters to the χ^2 value, thereby favoring simpler models when their χ^2 values are comparable. The corrected AIC (AIC_c) further refines this approach by including a correction term that accounts for small sample sizes, helping to prevent overfitting in cases where the number of data points is limited. The best-fit model is determined by minimizing the AIC_c score: lower AIC_c values indicate a better fit. Deviations between models are assessed using Jeffreys’ scale, where a difference $\Delta\text{AIC}_c > 5$ (10) is considered strong (decisive) evidence against the model with the higher AIC_c score.

5 Results and discussion

The cosmological analysis involves fitting the ICG and TICG models to two dataset combinations: BAO/CMB+H+RSD, and this combination augmented with the SN dataset. For comparison, we also include the analysis of the Λ CDM model. The resulting parameter constraints at the 68% CL, the χ^2 statistics and AIC_c are summarized in Tables 3 and 4. In Figures 1 ~ 3 we show the 1-D marginalized posterior distributions and 2-D joint contours at 1σ and 2σ CL.

The results outlined in Table 3 for BAO/CMB+H+RSD datasets offer significant insights. The initial conditions r_{i1} and r_{i2} reported at 68% CL are obtained for $\Omega_r^{(i)} = 0.9999929$ at $z = 4.85 \times 10^8$. We observe that the mean value at 68% CL of H_0 reported for the ICG and TICG, respectively, are higher than that reported for Λ CDM. This is significant in light of addressing the tension between the Planck-inferred value $H_0 = 67.4 \pm 0.5$ km/s/Mpc [7]

¹<https://github.com/cmbant/getdist>

and the locally measured value $H_0 = 74.03 \pm 1.42$ km/s/Mpc by Riess et al. [47, 48], indicating a reduction in tension to less than 1σ . Our results for σ_8 indicate that the mean values for the ICG and TICG are about 0.5σ lower than that of Λ CDM model. It can be said that the Λ CDM and the ICG and TICG models are in perfect agreement with the results of low-redshift observations and the σ_8 value inferred by Planck. However, the ICG model produced an S_8 value very close to that reported by the concordance model, thereby maintaining the tension with LSS observations by DES-Y3 [49]. In contrast, the TICG model yielded a much lower value that aligns well with LSS observations, at 0.4σ from DES-Y3 [49]. The discrepancy between the two solutions arises primarily because ICG allows for a higher value of $\Omega_m^{(0)}$, while TICG accommodates a smaller value compared to that of Λ CDM. The findings for the TICG model are consistent with the observation that the quantity $\Omega_m^{(0)} h^2$ is tightly constrained by Planck. Additionally, the existence of energy transfer from DE to DM suggests that the contribution from DM density needs to be reduced. Specifically, for negative α , the DM density receives an additional contribution proportional to the DE density.

Furthermore, the present day DE EoS lies within the phantom regime at 68% CL, with $w_0 = -1.2 \pm 0.01$ for ICG and $w_0 = -1.18_{-0.0060}^{+0.0069}$ for TICG, respectively. These values correlate with higher expansion rates, as illustrated in Fig. 1. This is true if we impose consistency with CMB observations. Indeed, the positions of the acoustic peaks in the CMB are influenced by the overall distance that light can travel from the surface of last scattering to us. When w is allowed to vary into the phantom region, the faster expansion due to $w < -1$ requires an increased H_0 to keep the acoustic peak positions unchanged. Moreover, the DM-DE coupling parameter exhibits mean values given by $\alpha = -0.101_{-0.019}^{+0.022}$ (ICG) and $\alpha = -0.071 \pm 0.0043$ (TICG) at 68% CL. This complex interplay between α , w_0 and H_0 can be observed in figures 1 and 2, where a strong degeneracy between α and w_{DE} dominate the one between α and H_0 in the ICG model.

Similarly, according to the results in Table 4, the parameter space becomes more constrained with the inclusion of SN data. For the entire dataset, including BAO/CMB+H+RSD and SN, the best fit initial conditions allowed for $\Omega_r^{(i)} = 0.9999929$ at $z = 4.85 \times 10^8$ are slightly reduced for ICG and TICG compared to the experiment with the BAO/CMB+H+RSD dataset. Specifically, $H_0 = 72 \pm 1.5$ km/s/Mpc and $H_0 = 72.8 \pm 1.7$ km/s/Mpc at a 68% CL for ICG and TICG, respectively. These values remain larger than those predicted by the Λ CDM model, reducing the tension with the value reported by SH0ES (R19) [47, 48] to 0.5σ and 0.1σ for ICG and TICG, respectively.

Additionally, the inclusion of SN data leads to a decrease in σ_8 for the ICG and TICG models, while it causes an increase in σ_8 for the Λ CDM model. Concurrently, an increase in $\Omega_m^{(0)}$ is observed for both ICG and TICG, similar to the scenario observed in the non-interacting covariant Galileon model [81]. As a result, the tension in S_8 for the ICG model increases to approximately 1σ , while it is alleviated in the TICG model to around 0.2σ from DES-Y3 data.

Moreover, a non-zero coupling constant, $\alpha = -0.128_{-0.0087}^{+0.0250}$ and $\alpha = -0.0614 \pm 0.0043$ at a 68% CL for ICG and TICG, respectively, is also obtained. In the ICG model, the negative increase in α is accompanied by a substantial decrease in w_0 and an increase in $\Omega_0^{(0)}$, driven by the energy transfer from DE to DM, and a shift in H_0 towards smaller values. In contrast, the TICG model shows an increase in the DM-DE coupling, accompanied by an increase in $\Omega_0^{(0)}$, and a decrease in w_0 and H_0 . Additionally, the significant decrease in the Hubble constant is crucial for maintaining $\Omega_m^{(0)} h^2$ nearly constant. However, the inclusion of the SN data does

not mitigate the tension with LSS observations; it remains at the same level as observed in the experiment without SN data.

For the two experiments, we observe that ICG exhibits a robust correlation between α and w_0 , meaning that the phantom regime is enhanced by the DM-DE interaction. In ICG, the resolution of the H_0 tension is driven by the phantom regime, while the S_8 tension is not resolved and remains at the level observed in Λ CDM, as seen in Fig. 1. For TICG, we observe in Fig. 2 that α and h are anti-correlated, while α and S_8 are correlated, explaining why both the H_0 and S_8 tensions are alleviated within the TICG solution. Finally, we observe that the 1-D posterior distributions feature narrow peaks comfortably situated within the permissible range defined by the priors, suggesting that the outcomes are not overly reliant on the selected parameters.

Moreover, the ICG model is free from the strong degeneracy between the parameters α and $\Omega_m^{(0)}$, observed in TICG. Importantly, the ICG and TICG models are free from non-adiabatic instabilities at large scales. This is evidenced by the doom factor, expressed as $d = -Q/(3\rho_x(1+w_x))$, being consistently negative [82].

A summary of our results can be drawn from Fig. 3. We clearly observe a shift in the current expansion rate towards higher values for both the ICG and TICG models compared to Λ CDM, alleviating the current tension between early and late-time observations. Specifically, we observe an excess in the current DM density for the ICG model, and a shift of S_8 to smaller values for the TICG model, which further alleviates the tension on S_8 . According to the values of AIC_c in Tables 3 and 4, the ICG model is slightly disfavored compared to Λ CDM, whereas the TICG model and Λ CDM are consistent with each other. Overall, the inclusion of SN data reveals significant dynamics in the interplay between cosmological parameters, underscoring the robustness of the ICG and TICG models in addressing various cosmological tensions while remaining stable at large scales.

Parameter	BAO/CMB+H+RSD		
	ICG $\chi_{min}^2 = 23.0529$	TICG $\chi_{min}^2 = 23.1082$	Λ CDM $\chi_{min}^2 = 22.8345$
α	$-0.101(-0.076)_{-0.019}^{+0.022}$	$-0.0711(-0.07) \pm 0.0043$	–
$10^{12}r_{1i}$	$0.093(0.095)_{-0.065}^{+0.089}$	–	–
$10^{18}r_{2i}$	$7.6(10.11)_{-1.8}^{+2.8}$	$(16.03(16.34)_{-0.49}^{+0.41}) \times 10^{-43}$	–
$\Omega_m^{(0)}$	0.31(0.30) \pm 0.013	0.28(0.277)_{-0.011}^{+0.010}	0.3016(0.302) \pm 0.0112
h	0.728(0.738) \pm 0.017	0.741(0.741) \pm 0.016	0.6896(0.688) \pm 0.0142
w	-1.2(-1.19) \pm 0.01	-1.18(-1.176)_{-0.0060}^{+0.0069}	-1
σ_8	0.791(0.784) \pm 0.031	0.79(0.797) \pm 0.03	0.811(0.81) \pm 0.0278
S_8	0.805(0.788) \pm 0.033	0.763(0.766) \pm 0.03	0.813(0.812) \pm 0.043
$\Delta\chi^2$	0.2184	0.2737	–
ΔAIC_c	4.8313	2.5423	–

Table 3: Mean values at 1σ CL for the ICG, TICG and the Λ CDM models for the combination BAO/CMB+H+RSD. The derived parameters are shown in bold, and in red we show the best fit values.

BAO/CMB+H+RSD+SN			
Parameter	ICG	TICG	Λ CDM
	$\chi^2_{min} = 29.1583$	$\chi^2_{min} = 29.223$	$\chi^2_{min} = 28.4213$
α	$-0.128(-0.111)_{-0.0087}^{+0.025}$	$-0.0614(-0.06) \pm 0.0043$	—
$10^{12}r_{1z}$	$0.05(0.063)_{-0.021}^{+0.019}$	—	—
$10^{18}r_{2z}$	$4.3(3.9)_{-1.2}^{+2.2}$	$(15.53(15.73) \pm 0.14) \times 10^{-43}$	—
$\Omega_m^{(0)}$	0.337(0.331) \pm 0.012	0.307(0.308) $_{-0.013}^{+0.014}$	$0.301(0.302) \pm 0.0111$
h	$0.72(0.722) \pm 0.015$	$0.728(0.728) \pm 0.017$	$0.691(0.688) \pm 0.014$
w	$-1.224(-1.22)_{-0.0092}^{+0.0110}$	$-1.1953(-1.196)_{-0.0071}^{+0.0083}$	-1
σ_8	$0.776(0.776) \pm 0.032$	$0.775(0.778)_{-0.025}^{+0.029}$	$0.812(0.809) \pm 0.029$
S_8	0.823(0.816) \pm 0.037	0.783(0.788) \pm 0.029	0.812(0.813) \pm 0.03
$\Delta\chi^2$	0.737	0.8017	—
ΔAIC_c	5.35	3.07	—

Table 4: Mean values at 1σ CL for the ICG, TICG and the Λ CDM models for the full dataset BAO/CMB+H+RSD+SN. The derived parameters are shown in bold and the best fit values in red.

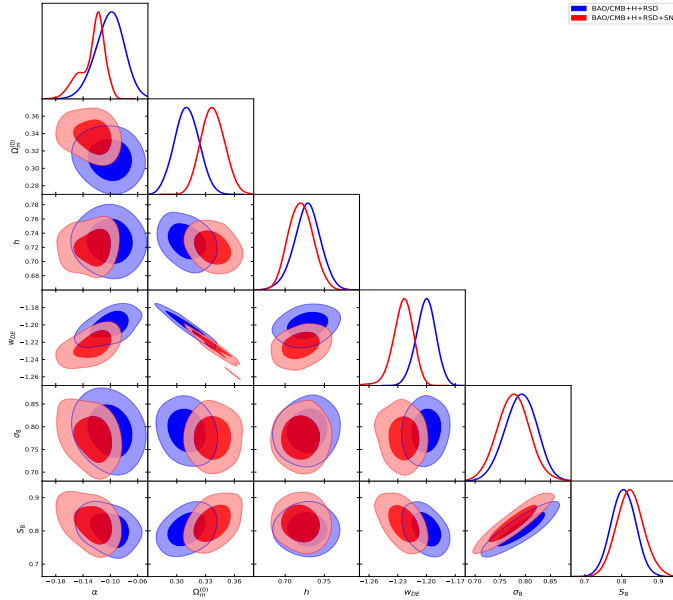


Figure 1: One-dimensional marginalized posterior distributions and two-dimensional joint contours at 1σ and 2σ confidence levels for the BAO/CMB+H+RSD (light blue) and BAO/CMB+H+RSD+SN (orange) datasets for the ICG model.

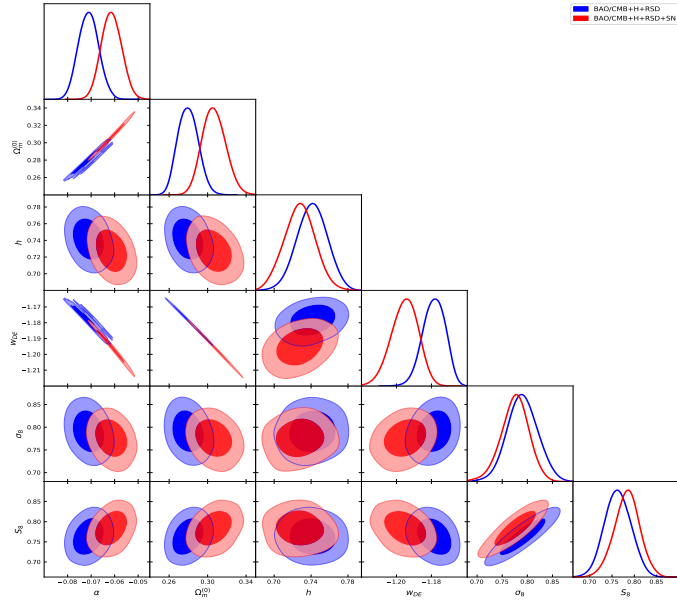


Figure 2: One-dimensional marginalized posterior distributions and two-dimensional joint contours at 1σ and 2σ confidence levels for the BAO/CMB+H+RSD (light blue) and BAO/CMB+H+RSD+SN (orange) datasets for the TICG model.

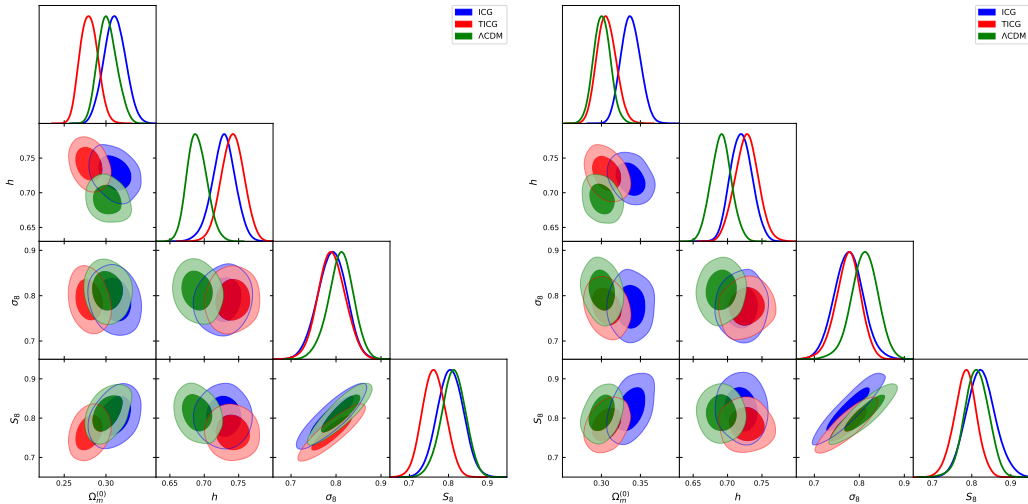


Figure 3: 1-D marginalized posterior and 2-D joint contours at 1σ and 2σ CL of various models for dataset BAO/CMB+H+RSD (left panel), and the entire dataset BAO/CMB+H+RSD+SN (right panel).

In the left panel of Fig. 4, we plot the EoS of DE, w_x , for the combination of the full datasets, using the best fit values of the initial conditions r_{i1} and r_{i2} . As illustrated in this figure, the DE EoS in TICG always remains in the phantom regime. In ICG, it undergoes a rapid transition around the epoch of matter-radiation equality, which occurs at $z_{eq} \simeq 3380$ using the best fit parameters. It then stays constant at the onset of the time of recombination

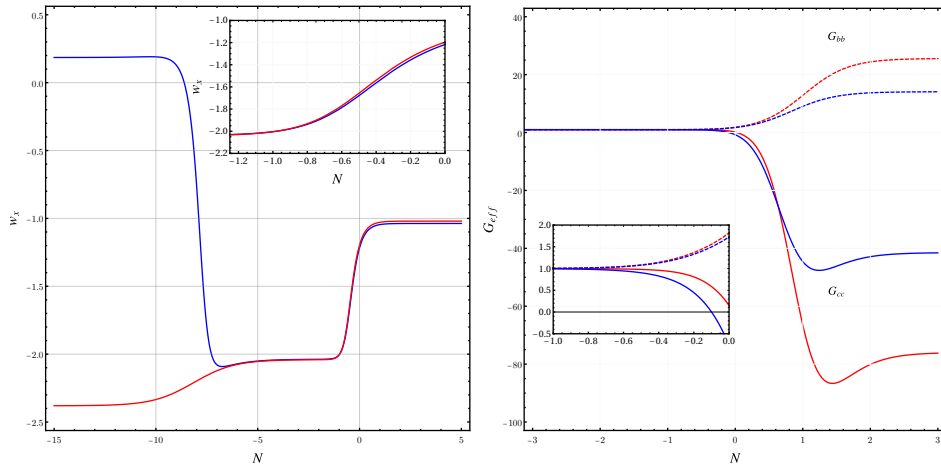


Figure 4: Left: Evolution of the EoS of DE vs N (right panel). Right: The effective gravitational constants G_{cc} (solid lines), and G_{bb} (dashed lines). In both panels we use the best fit parameters for ICG (in blue) and TICG (in red) for the combination BAO/CMB+H+RSD+SN.

before undergoing a second rapid transition around $z_t \sim 1$. This evolution in the phantom regime has strong impact on H_0 and $f\sigma_8$, as has been confirmed above. This scenario, first discovered in the Covariant Galileon field [83], is also consistent with the transitional dark energy (TDE) scenario [84, 85]. In the right panel, the evolution of the effective gravitational constants G_{cc} and G_{bb} with redshift is plotted using the best fit parameters. We observe that for both the ICG and TICG models, the effective gravitational coupling G_{cc} during the DE-dominated era is smaller than unity starting approximately from the transitional redshift at z_t , and even becomes negative near the present time. This latter behavior may lead to slower structural growth in TICG; however, it is significantly more pronounced in ICG, resulting in markedly reduced growth rates. In contrast, the baryon-baryon effective coupling G_{bb} follows the opposite trend.

In Figure 5, we present the theoretical predictions for $H(z)/(1+z)$ derived from the combination of the full datasets. We showcase the best-fit projections for ICG, TICG, and Λ CDM models, alongside Λ CDM with Planck 18 data, juxtaposed with the DESI Collaboration measurements [86], BOSS DR12 [87], BOSS DR14 quasars [88], and BOSS DR14 Lyman- α forest [89, 90] data points. Notably, the ICG and TICG models demonstrate a better fit to $H(z)$ for the data reported by DESI Collaboration, compared to Λ CDM. The anomaly in the data point at $z = 0.51$ has recently been addressed [91], while waiting for the future data that will be provided by the DESI Collaboration. For the remaining non-DESI data, we observe the same mediocre fit for all models. Moreover, ICG and TICG predict a higher present day expansion rate H_0 , evident in the disparity between the red and blue curves compared to the black curves at $z = 0$. The consistent behaviors illustrated in Figure 5 during later times for the ICG and TICG models, beginning from the DM-DE equality, are attributed to the shared de Sitter attractor present in both models at those stages. We also observe the crossing of the ICG and TICG curves through the Λ CDM curve at the redshift of DM-DE equality $z \sim 0.3$, and $z_t \sim 1$, where the rapid transition of the DE EoS occurs.

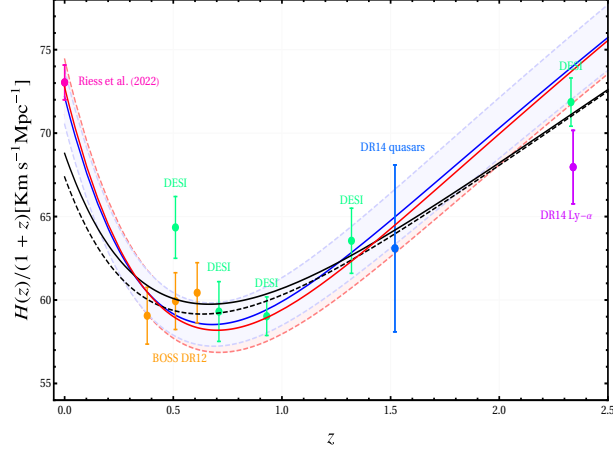


Figure 5: Redshift evolution of $H(z)/(1+z)$ for the full combination of datasets. Data points of local measurements by Riess et al.[33] (for H_0), BOSS DR12 [87], BOSS DR14 quasars [88], BOSS DR14 Ly- α [89, 90], and DESI 2024 [86] are shown. The Blue, red, black and black dashed curves are for the ICG, TICG, the best fit Λ CDM and Λ CDM with Planck 18, respectively.

Let us now use an other diagnostic to asses the quality of our results regarding the latest BAO release provided by the DESI collaboration [86]. This diagnostic used the quantity defined as [92]

$$A(z) = \frac{D_M(z)}{zD_H(z)}, \quad (5.1)$$

where

$$D_M(z) = \frac{c}{H_0} \int_0^z \frac{dz'}{E(z')}, \quad D_H(z) = \frac{c}{E(z)}, \quad (5.2)$$

are the transverse and line-of-sight comoving distances, respectively, and $E(z)$ is the normalized Hubble parameter $H(z) = H_0 E(z)$. The notable feature of $A(z)$ lies in its independence from the sound horizon at the baryon drag epoch r_d . This property facilitates the computation of $A(z)$ if $E(z)$ is known. In Figure 6, we clearly observe that the $A(z)$ curves for the ICG and TICG models are indistinguishable and provide an excellent fit to the DESI BAO data [86], with the notable exception of the anomalous data point at $z = 0.51$. Compared to the flat Λ CDM model, we observe significant evidence for dynamical phantom regime. An other consequence of the particular behavior of the EoS of DE is reflected in the crossing of the Λ CDM curve at redshift $z \sim z_t$. The observed degeneracy between ICG and TICG concerning the $A(z)$ -test suggests that this evaluation alone might not suffice for effectively discriminating between different models.

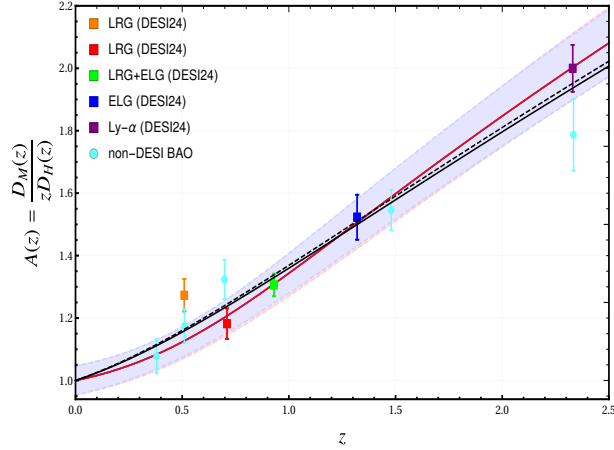


Figure 6: In Figure 6, we present $A(z)$ versus z for the full dataset. The ICG and TICG curves (in blue and red, respectively) are indistinguishable, while the Λ CDM model is shown with the best fit results in a solid black curve and with the Planck 18 data in a dashed black curve. Data points and their 1σ errors are listed in Tables 1 and 4 in [93]

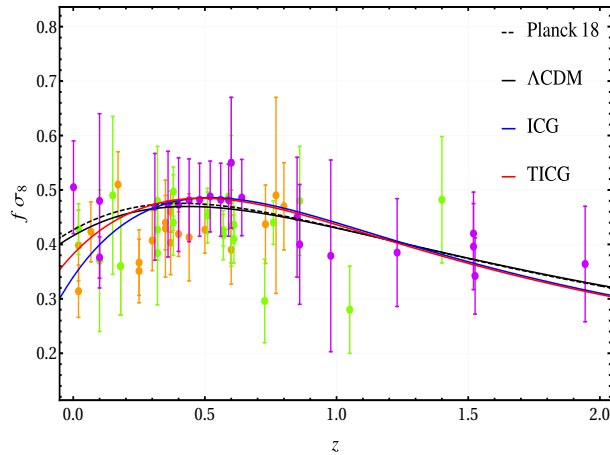


Figure 7: Redshift evolution of $f\sigma_8(z)$ for the full combination of datasets. The observational data are for the 21 latest (Violet), earliest (Orange) and the remaining (Green) data points taken from the Table in Appendix A. The black and the black dashed curves are the best fit Λ CDM and Λ CDM with Planck 18, respectively.

In Figure 7, we plot the best-fit behavior of $f\sigma_8$ for the ICG and TICG models, comparing them to the best-fit Planck 18 Λ CDM model. The ICG and TICG models are indistinguishable before the DM-DE equality epoch $a \sim 0.3$, and exhibit less growth than in the Λ CDM model and Planck data in the present epoch, starting at the DM-DE equality redshift. This behavior can be attributed to the weaker effective gravitational constant, essentially due to G_{cc} for the ICG model. An interesting pattern emerges from Figures 5 and 7. Specifically, we observe two transition redshifts at $z \sim 0.3$ and $z \sim z_t$, where the Hubble parameter and the rate of structure growth in the ICG and TICG models deviate from those in the Λ CDM model. This

behavior is related to the particular evolution of the EoS of DE and the effective gravitational constants, particularly G_{cc} as illustrated in figure 4. Notably, for $0.3 \lesssim z \lesssim z_t$, the growth rate of structures in ICG and TICG closely matches the latest RSD measurements (depicted in violet) with remarkable precision, similar to how $H(z)$ and $A(z)$ correspond closely to measurements obtained by the DESI Collaboration [86]. We note that, even though we used only the recently published RSD data in our study, our results remain consistent with the full set of data presented in the Table in appendix A. The decline in the growth rate of structures reported by ICG is notably sharper compared to both TICG and Λ CDM, essentially attributed to the negative trend of G_{cc} beyond $z > 0.3$. Meanwhile, the rate of structure growth in TICG decreases moderately in contrast to Λ CDM. This latter observation elucidates why the tension on S_8 between Planck and LSS observations is entirely alleviated within the TICG model.

6 Conclusions

In this study, we explored the richness of interacting dark energy and dark matter cosmology in the framework of the cubic covariant Galileon model, and its efficacy in addressing the enduring and notably significant H_0 and S_8 tensions. Our investigation focused on an interaction term proportional to the Hubble parameter and Galileon dark energy, expressed as $Q = \alpha H \rho_x$. By initially considering the existence of a de Sitter (dS) cosmological era, we were able to express the free parameters in the Galileon Lagrangian in terms of the coupling constant, thus reducing the dimensionality of the parameter space. Utilizing appropriate dimensionless variables and transforming the field equations into an autonomous system of first-order differential equations, we conducted a comprehensive dynamical system analysis. This analysis revealed the typical physical phase space, encompassing various cosmological epochs such as radiation domination, matter domination, and dark energy domination, ultimately leading to a de Sitter expansion in the future.

The identification of a stable attractor in the dS era enabled the construction of an approximated tracking solution, closely mimicking the exact solution, particularly in the recent past before reaching the dS era. Notably, along the tracker solution, the dark energy equation of state exhibited distinctive behaviors corresponding to different cosmological epochs, showing particularly a transitional behavior as the one observed in transitional dark energy models (TDE), and first observed in the interacting covariant Galileon field.

Transitioning to the analysis of parameter constraints for the exact solution (ICG), the approximate tracker solution (TICG), and the Λ CDM model, our results provided valuable insights. Our examination of the BAO/CMB+H+RSD and BAO/CMB+H+RSD+SN combinations revealed a preference for a phantom regime in both solutions. We found that the current cosmological tensions on H_0 and S_8 are alleviated at the 68% confidence level within the TICG solution. This alleviation is attributed to the observed anti-correlation between the DM-DE coupling constant α and the Hubble constant H_0 , and the correlation between α and S_8 . This suggests that the cosmological tensions within TICG are driven by the interaction between dark matter and dark energy, while in ICG, the resolution of the H_0 tension is driven by the phantom regime.

In summary, our study advances our understanding of the complex dynamics within the interacting cubic covariant Galileon model. We emphasize the importance of the tracker solution, which emerges as a compelling avenue for addressing the H_0 and S_8 tensions. While frequentist evidence analysis favors the Λ CDM model over the ICG and TICG solutions, our

findings underscore the potential of this model to provide valuable insights into some of the foremost challenges in modern cosmology.

Acknowledgments

KN was financially supported by the Algerian Ministry of Higher Education and Scientific Research (MESRS).

References

- [1] G. Bertone, D. Hooper and J. Silk, *Particle dark matter: Evidence, candidates and constraints*, *Physics reports* **405** (2005) 279 [[hep-ph/0404175](#)].
- [2] J. Silk et al., *Particle Dark Matter: Observations, Models and Searches*, Cambridge Univ. Press, Cambridge (2010).
- [3] A.G. Riess and et al, *Observational evidence from supernovae for an accelerating universe and a cosmological constant*, *The astronomical journal* **116** (1998) 1009 [[astro-ph/9805201](#)].
- [4] S. Perlmutter and et al, *Measurements of Ω and Λ from 42 high-redshift supernovae*, *The Astrophysical Journal* **517** (1999) 565 [[astro-ph/9812133](#)].
- [5] D.N. Spergel and et al, *First-year Wilkinson Microwave Anisotropy Probe (WMAP) observations: determination of cosmological parameters*, *The Astrophysical Journal Supplement Series* **148** (2003) 175 [[astro-ph/0302209](#)].
- [6] G. Hinshaw and et al, *Nine-year Wilkinson Microwave Anisotropy Probe (WMAP) observations: cosmological parameter results*, *The Astrophysical Journal Supplement Series* **208** (2013) 19 [[1212.5226](#)].
- [7] N. Aghanim, Y. Akrami, M. Ashdown, J. Aumont, C. Baccigalupi, M. Ballardini et al., *Planck 2018 results-VI. Cosmological parameters*, *Astronomy & Astrophysics* **641** (2020) A6 [[1807.06209](#)].
- [8] E.J. Copeland, M. Sami and S. Tsujikawa, *Dynamics of dark energy*, *International Journal of Modern Physics D* **15** (2006) 1753 [[hep-th/0603057](#)].
- [9] S.M. Carroll, *The cosmological constant*, *Living reviews in relativity* **4** (2001) 1 [[astro-ph/0004075](#)].
- [10] P. Bull, Y. Akrami, J. Adamek, T. Baker, E. Bellini, J.B. Jimenez et al., *Beyond Λ CDM: Problems, solutions, and the road ahead*, *Physics of the Dark Universe* **12** (2016) 56 [[1512.05356](#)].
- [11] L. Perivolaropoulos and F. Skara, *Challenges for Λ CDM: An update*, *New Astronomy Reviews* **95** (2022) 101659 [[2105.05208](#)].
- [12] S. Weinberg, *The cosmological constant problem*, *Rev. Mod. Phys.* **61** (1989) 1.
- [13] H.E. Velten, R. Vom Marttens and W. Zimdahl, *Aspects of the cosmological coincidence problem*, *The European Physical Journal C* **74** (2014) 1 [[1410.2509](#)].
- [14] S. Tsujikawa, *Dark energy: investigation and modeling*, in *Dark Matter and Dark Energy: A Challenge for Modern Cosmology*, pp. 331–402, Springer (2011) [[1004.1493](#)].
- [15] Y. Fujii, *Origin of the gravitational constant and particle masses in a scale-invariant scalar-tensor theory*, *Phys. Rev. D* **26** (1982) 2580.
- [16] L.H. Ford, *Cosmological-constant damping by unstable scalar fields*, *Phys. Rev. D* **35** (1987) 2339.

- [17] C. Wetterich, *Cosmology and the fate of dilatation symmetry*, *Nuclear Physics B* **302** (1988) 668.
- [18] R.R. Caldwell, R. Dave and P.J. Steinhardt, *Cosmological imprint of an energy component with general equation of state*, *Physical Review Letters* **80** (1998) 1582 [[astro-ph/9708069](#)].
- [19] I. Zlatev, L. Wang and P.J. Steinhardt, *Quintessence, cosmic coincidence, and the cosmological constant*, *Physical Review Letters* **82** (1999) 896 [[astro-ph/9807002](#)].
- [20] S. Tsujikawa, *Quintessence: a review*, *Classical and Quantum Gravity* **30** (2013) 214003 [[1304.1961](#)].
- [21] C. Armendariz-Picon, V. Mukhanov and P.J. Steinhardt, *Dynamical solution to the problem of a small cosmological constant and late-time cosmic acceleration*, *Physical Review Letters* **85** (2000) 4438 [[astro-ph/0004134](#)].
- [22] T. Padmanabhan, *Accelerated expansion of the universe driven by tachyonic matter*, *Physical Review D* **66** (2002) 021301 [[hep-th/0204150](#)].
- [23] T. Padmanabhan and T.R. Choudhury, *Can the clustered dark matter and the smooth dark energy arise from the same scalar field?*, *Physical Review D* **66** (2002) 081301 [[hep-th/0205055](#)].
- [24] A. Kamenshchik, U. Moschella and V. Pasquier, *An alternative to quintessence*, *Physics Letters B* **511** (2001) 265 [[gr-qc/0103004](#)].
- [25] N. Bilić, G.B. Tupper and R.D. Viollier, *Unification of dark matter and dark energy: the inhomogeneous Chaplygin gas*, *Physics Letters B* **535** (2002) 17 [[astro-ph/0111325](#)].
- [26] M. Bento, O. Bertolami and A.A. Sen, *Generalized Chaplygin gas, accelerated expansion, and dark-energy-matter unification*, *Physical Review D* **66** (2002) 043507 [[gr-qc/0202064](#)].
- [27] T. Clifton, P.G. Ferreira, A. Padilla and C. Skordis, *Modified gravity and cosmology*, *Physics reports* **513** (2012) 1 [[1106.2476](#)].
- [28] S. Nojiri, S. Odintsov and V. Oikonomou, *Modified gravity theories on a nutshell: Inflation, bounce and late-time evolution*, *Physics Reports* **692** (2017) 1 [[1705.11098](#)].
- [29] E.N. Saridakis, R. Lazkoz, V. Salzano, P.V. Moniz, S. Capozziello, J.B. Jiménez et al., *Modified gravity and cosmology*, Springer (2021).
- [30] I. Quiros, *Selected topics in scalar–tensor theories and beyond*, *International Journal of Modern Physics D* **28** (2019) 1930012 [[1901.08690](#)].
- [31] A. Nicolis, R. Rattazzi and E. Trincherini, *Galileon as a local modification of gravity*, *Physical Review D* **79** (2009) 064036 [[0811.2197](#)].
- [32] T. Kobayashi, *Horndeski theory and beyond: a review*, *Reports on Progress in Physics* **82** (2019) 086901 [[1901.07183](#)].
- [33] C. Deffayet and D.A. Steer, *A formal introduction to Horndeski and Galileon theories and their generalizations*, *Classical and Quantum Gravity* **30** (2013) 214006 [[1307.2450](#)].
- [34] C. Deffayet, G. Esposito-Farese and A. Vikman, *Covariant galileon*, *Physical Review D* **79** (2009) 084003 [[0901.1314](#)].
- [35] C. Deffayet, S. Deser and G. Esposito-Farese, *Generalized Galileons: All scalar models whose curved background extensions maintain second-order field equations and stress tensors*, *Physical Review D* **80** (2009) 064015 [[0906.1967](#)].
- [36] G. Dvali, G. Gabadadze and M. Porrati, *4D gravity on a brane in 5D Minkowski space*, *Physics Letters B* **485** (2000) 208 [[hep-th/0005016](#)].
- [37] M.A. Luty, M. Porrati and R. Rattazzi, *Strong interactions and stability in the DGP model*, *Journal of High Energy Physics* **2003** (2003) 029 [[hep-th/0303116](#)].

- [38] A. Nicolis and R. Rattazzi, *Classical and quantum consistency of the DGP model*, *Journal of High Energy Physics* **2004** (2004) 059 [[hep-th/0404159](#)].
- [39] T. Kobayashi, M. Yamaguchi and J. Yokoyama, *Inflation driven by the Galileon field*, *Physical review letters* **105** (2010) 231302 [[1008.0603](#)].
- [40] C. Burrage, C. de Rham, D. Seery and A.J. Tolley, *Galileon inflation*, *Journal of Cosmology and Astroparticle Physics* **2011** (2011) 014 [[1009.2497](#)].
- [41] C. Deffayet, O. Pujolas, I. Sawicki and A. Vikman, *Imperfect dark energy from kinetic gravity braiding*, *Journal of Cosmology and Astroparticle Physics* **2010** (2010) 026 [[1008.0048](#)].
- [42] N. Chow and J. Khoury, *Galileon cosmology*, *Physical Review D* **80** (2009) 024037 [[0905.1325](#)].
- [43] F.P. Silva and K. Koyama, *Self-accelerating universe in Galileon cosmology*, *Physical Review D* **80** (2009) 121301 [[0909.4538](#)].
- [44] T. Kobayashi, *Cosmic expansion and growth histories in Galileon scalar-tensor models of dark energy*, *Physical Review D* **81** (2010) 103533 [[1003.3281](#)].
- [45] C. Charmousis, E.J. Copeland, A. Padilla and P.M. Saffin, *General second-order scalar-tensor theory and self-tuning*, *Physical Review Letters* **108** (2012) 051101 [[1106.2000](#)].
- [46] E.J. Copeland, A. Padilla and P.M. Saffin, *The cosmology of the Fab-Four*, *Journal of Cosmology and Astroparticle Physics* **2012** (2012) 026 [[1208.3373](#)].
- [47] A.G. Riess, W. Yuan, L.M. Macri, D. Scolnic, D. Brout, S. Casertano et al., *A Comprehensive Measurement of the Local Value of the Hubble Constant with $1 \text{ km s}^{-1} \text{ Mpc}^{-1}$ Uncertainty from the Hubble Space Telescope and the SH0ES Team*, *The Astrophysical Journal Letters* **934** (2022) L7.
- [48] Y.S. Murakami, A.G. Riess, B.E. Stahl, W. D’Arcy Kenworthy, D.-M.A. Pluck, A. Macoreтта et al., *Leveraging SN Ia spectroscopic similarity to improve the measurement of H_0* , *Journal of Cosmology and Astroparticle Physics* **2023** (2023) 046 [[2306.00070](#)].
- [49] T.M.C. Abbott, M. Aguena, A. Alarcon, S. Allam, O. Alves, A. Amon et al., *Dark Energy Survey Year 3 results: Cosmological constraints from galaxy clustering and weak lensing*, *Phys. Rev. D* **105** (2022) 023520 [[2105.13549](#)].
- [50] B. Wang, E. Abdalla, F. Atrio-Barandela and D. Pavon, *Dark matter and dark energy interactions: theoretical challenges, cosmological implications and observational signatures*, *Reports on Progress in Physics* **79** (2016) 096901 [[1603.08299](#)].
- [51] E. Di Valentino, A. Melchiorri and O. Mena, *Can interacting dark energy solve the H_0 tension?*, *Physical Review D* **96** (2017) 043503 [[1704.08342](#)].
- [52] M.A. Buen-Abad, M. Schmaltz, J. Lesgourgues and T. Brinckmann, *Interacting dark sector and precision cosmology*, *Journal of Cosmology and Astroparticle Physics* **2018** (2018) 008 [[1708.09406](#)].
- [53] W. Yang, S. Pan, E. Di Valentino, R.C. Nunes, S. Vagnozzi and D.F. Mota, *Tale of stable interacting dark energy, observational signatures, and the H_0 tension*, *Journal of Cosmology and Astroparticle Physics* **2018** (2018) 019 [[1805.08252](#)].
- [54] W. Yang, A. Mukherjee, E. Di Valentino and S. Pan, *Interacting dark energy with time varying equation of state and the H_0 tension*, *Physical Review D* **98** (2018) 123527 [[1805.08252](#)].
- [55] S. Pan, W. Yang, C. Singha and E.N. Saridakis, *Observational constraints on sign-changeable interaction models and alleviation of the H_0 tension*, *Physical Review D* **100** (2019) 083539 [[1903.10969](#)].
- [56] W. Yang, O. Mena, S. Pan and E. Di Valentino, *Dark sectors with dynamical coupling*, *Physical Review D* **100** (2019) 083509 [[1906.11697](#)].

- [57] S. Pan, W. Yang, E. Di Valentino, E.N. Saridakis and S. Chakraborty, *Interacting scenarios with dynamical dark energy: observational constraints and alleviation of the H_0 tension*, *Physical Review D* **100** (2019) 103520 [[1907.07540](#)].
- [58] M. Martinelli, N.B. Hogg, S. Peirone, M. Bruni and D. Wands, *Constraints on the interacting vacuum-geodesic CDM scenario*, *Monthly Notices of the Royal Astronomical Society* **488** (2019) 3423 [[1902.10694](#)].
- [59] S. Pan, W. Yang and A. Paliathanasis, *Non-linear interacting cosmological models after Planck 2018 legacy release and the H_0 tension*, *Monthly Notices of the Royal Astronomical Society* **493** (2020) 3114 [[2002.03408](#)].
- [60] W. Yang, S. Pan, E. Di Valentino, O. Mena and A. Melchiorri, *2021- H_0 odyssey: closed, phantom and interacting dark energy cosmologies*, *Journal of Cosmology and Astroparticle Physics* **2021** (2021) 008 [[2101.03129](#)].
- [61] W. Yang, S. Pan, O. Mena and E. Di Valentino, *On the dynamics of a dark sector coupling*, *Journal of High Energy Astrophysics* **40** (2023) 19 [[2209.14816](#)].
- [62] S. Kumar, R.C. Nunes and S.K. Yadav, *Dark sector interaction: a remedy of the tensions between CMB and LSS data*, *The European Physical Journal C* **79** (2019) 576 [[1903.04865](#)].
- [63] A. Pourtsidou and T. Tram, *Reconciling CMB and structure growth measurements with dark energy interactions*, *Physical Review D* **94** (2016) 043518 [[1604.04222](#)].
- [64] R. An, C. Feng and B. Wang, *Relieving the tension between weak lensing and cosmic microwave background with interacting dark matter and dark energy models*, *Journal of Cosmology and Astroparticle Physics* **2018** (2018) 038 [[1711.06799](#)].
- [65] C. Van De Bruck and J. Mifsud, *Searching for dark matter-dark energy interactions: going beyond the conformal case*, *Physical Review D* **97** (2018) 023506 [[1709.04882](#)].
- [66] S.M. Carroll, *Quintessence and the rest of the world: suppressing long-range interactions*, *Physical Review Letters* **81** (1998) 3067 [[astro-ph/9806099](#)].
- [67] O. Bertolami, F.G. Pedro and M. Le Delliou, *Dark energy-dark matter interaction and putative violation of the equivalence principle from the abell cluster A586*, *Physics Letters B* **654** (2007) 165 [[astro-ph/0703462](#)].
- [68] J. Valiviita, E. Majerotto and R. Maartens, *Large-scale instability in interacting dark energy and dark matter fluids*, *Journal of Cosmology and Astroparticle Physics* **2008** (2008) 020 [[0804.0232](#)].
- [69] A. De Felice and S. Tsujikawa, *Conditions for the cosmological viability of the most general scalar-tensor theories and their applications to extended Galileon dark energy models*, *Journal of Cosmology and Astroparticle Physics* **2012** (2012) 007 [[1110.3878](#)].
- [70] D.J. Holden and D. Wands, *Self-similar cosmological solutions with a nonminimally coupled scalar field*, *Physical Review D* **61** (2000) .
- [71] S. Nesseris, A. De Felice and S. Tsujikawa, *Observational constraints on Galileon cosmology*, *Physical Review D* **82** (2010) 124054 [[1010.0407](#)].
- [72] L. Perko, *Differential Equations and Dynamical Systems*, Texts in Applied Mathematics, Springer New York (2012).
- [73] N. Bartolo, E. Bellini, D. Bertacca and S. Matarrese, *Matter bispectrum in cubic Galileon cosmologies*, *Journal of Cosmology and Astroparticle Physics* **2013** (2013) 034 [[1301.4831](#)].
- [74] L. Kazantzidis and L. Perivolaropoulos, *Evolution of the $f\sigma_8$ tension with the determination Planck15/ Λ CDM and implications for modified gravity theories*, *Phys. Rev. D* **97** (2018) 103503 [[1803.01337](#)].

- [75] S. Nesseris, G. Pantazis and L. Perivolaropoulos, *Tension and constraints on modified gravity parametrizations of $G_{\text{eff}}(z)$ from growth rate and Planck data*, *Phys. Rev. D* **96** (2017) 023542 [[1703.10538](#)].
- [76] R. Jimenez and A. Loeb, *Constraining Cosmological Parameters Based on Relative Galaxy Ages*, *The Astrophysical Journal* **573** (2002) 37–42 [[0106145](#)].
- [77] M.V.d. Santos, R. Reis and I. Waga, *Constraining the cosmic deceleration-acceleration transition with type Ia supernova, BAO/CMB and $H(z)$ data*, *Journal of Cosmology and Astroparticle Physics* **2016** (2016) 066–066 [[1505.03814v2](#)].
- [78] A.G. Riess, S.A. Rodney, D.M. Scolnic, D.L. Shafer, L.-G. Strolger, H.C. Ferguson et al., *Type Ia Supernova Distances at Redshift > 1.5 from the Hubble Space Telescope Multi-cycle Treasury Programs: The Early Expansion Rate*, *The Astrophysical Journal* **853** (2018) 126 [[1710.00844v1](#)].
- [79] A. Lewis, *GetDist: a Python package for analysing Monte Carlo samples*, [1910.13970](#).
- [80] H. Akaike, *A New Look at the Statistical Model Identification*, *IEEE Transactions on Automatic Control* **19** (1974) 716.
- [81] S. Nesseris, A. de Felice and S. Tsujikawa, *Observational constraints on Galileon cosmology*, *Phys. Rev. D* **82** (2010) 124054 [[1010.0407](#)].
- [82] M.B. Gavela, D. Hernandez, L.L. Honorez, O. Mena and S. Rigolin, *Dark coupling*, *Journal of Cosmology and Astroparticle Physics* **2009** (2009) 034 [[0901.1611](#)].
- [83] A. De Felice and S. Tsujikawa, *Cosmology of a covariant Galileon field*, *Phys. Rev. Lett.* **105** (2010) 111301 [[1007.2700](#)].
- [84] Z. Zhou, G. Liu, Y. Mu and L. Xu, *Can phantom transition at $z \sim 1$ restore the Cosmic concordance?*, *Mon. Not. Roy. Astron. Soc.* **511** (2022) 595 [[2105.04258](#)].
- [85] R.E. Keeley, S. Joudaki, M. Kaplinghat and D. Kirkby, *Implications of a transition in the dark energy equation of state for the H_0 and σ_8 tensions*, *JCAP* **12** (2019) 035 [[1905.10198](#)].
- [86] DESI Collaboration: A. G. Adame, J. Aguilar, S. Ahlen, S. Alam, D.M. Alexander, M. Alvarez et al., *DESI 2024 VI: Cosmological Constraints from the Measurements of Baryon Acoustic Oscillations*, [2404.03002](#).
- [87] S. Alam, M. Ata, S. Bailey, F. Beutler, D. Bizyaev, J.A. Blazek et al., *The clustering of galaxies in the completed SDSS-III Baryon Oscillation Spectroscopic Survey: cosmological analysis of the DR12 galaxy sample*, *Monthly Notices of the Royal Astronomical Society* **470** (2017) 2617 [[1607.03155](#)].
- [88] P. Zarrouk, E. Burtin, H. Gil-Marín, A.J. Ross, R. Tojeiro, I. Pâris et al., *The clustering of the SDSS-IV extended Baryon Oscillation Spectroscopic Survey DR14 quasar sample: measurement of the growth rate of structure from the anisotropic correlation function between redshift 0.8 and 2.2*, *Monthly Notices of the Royal Astronomical Society* **477** (2018) 1639–1663 [[1801.03062](#)].
- [89] V. de Sainte Agathe, C. Balland, H. du Mas des Bourboux, N.G. Busca, M. Blomqvist, J. Guy et al., *Baryon acoustic oscillations at $z = 2.34$ from the correlations of Ly α absorption in eBOSS DR14*, *Astronomy & Astrophysics* **629** (2019) A85 [[1904.03400](#)].
- [90] M. Blomqvist, H. du Mas des Bourboux, N.G. Busca, V. de Sainte Agathe, J. Rich, C. Balland et al., *Baryon acoustic oscillations from the cross-correlation of Ly α absorption and quasars in eBOSS DR14*, *Astronomy & Astrophysics* **629** (2019) A86 [[1904.03430](#)].
- [91] E.O. Colgain, M.G. Dainotti, S. Capozziello, S. Pourojaghi, M.M. Sheikh-Jabbari and D. Stojkovic, *Does DESI 2024 Confirm Λ CDM ?*, [2404.08633](#).

- [92] E.O. Colgain, M.M. Sheikh-Jabbari, R. Solomon, G. Bargiacchi, S. Capozziello, M.G. Dainotti et al., *Revealing intrinsic flat Λ CDM biases with standardizable candles*, *Physical Review D* **106** (2022) L041301 [[2203.10558](#)].
- [93] B.R. Dinda, *A new diagnostic for the null test of dynamical dark energy in light of DESI 2024 and other BAO data*, [2405.06618](#).
- [94] Y. Song and W.J. Percival, *Reconstructing the history of structure formation using redshift distortions*, *Journal of Cosmology and Astroparticle Physics* **10** (2009) 004 [[0807.0810](#)].
- [95] C. Zhang et al., *Four New Observational $H(z)$ Data From Luminous Red Galaxies of Sloan Digital Sky Survey Data Release Seven*, *Res. Astron. Astrophys.* **14** (2014) 1221 [[1207.4541](#)].
- [96] M. Davis et al., *Local gravity versus local velocity: solutions for β and non-linear bias*, *Mon. Not. Roy. Astron. Soc.* **413** (2011) 2906 [[1011.3114](#)].
- [97] M.J. Hudson and S.J. Turnbull, *THE GROWTH RATE OF COSMIC STRUCTURE FROM PECULIAR VELOCITIES AT LOW AND HIGH REDSHIFTS*, *ApJL* **751** (2012) L30 [[1203.4814](#)].
- [98] J. Simon, L. Verde and R. Jimenez, *Constraints on the redshift dependence of the dark energy potential*, *Phys. Rev. D* **71** (2005) 123001 [[0412269](#)].
- [99] S.J. Turnbull et al., *Cosmic flows in the nearby universe from type Ia supernovae*, *Mon. Not. Roy. Astron. Soc.* **420** (2012) 447 [[1111.0631](#)].
- [100] M. Moresco et al., *Improved constraints on the expansion rate of the universe up to $z \sim 1.1$ from the spectroscopic evolution of cosmic chronometers*, *J. Cosmol. Astropart. Phys.* **8** (2012) 006 [[1201.3609](#)].
- [101] L. Samushia, W.J. Percival and A. Raccanelli, *Interpreting large-scale redshift-space distortion measurements*, *Mon. Not. Roy. Astron. Soc.* **420** (2012) 2102 [[1102.1014](#)].
- [102] C. Blake et al., *The WiggleZ Dark Energy Survey: Joint measurements of the expansion and growth history at $z < 1$* , *Mon. Not. Roy. Astron. Soc.* **425** (2012) 405 [[1204.3674](#)].
- [103] C.-H. Chuang et al., *Measurements of $H(z)$ and $D_A(z)$ from the two-dimensional two-point correlation function of sloan digital sky survey luminous red galaxies*, *Mon. Not. R. Astron. Soc.* **426** (2012) 226 [[1102.2251](#)].
- [104] M. Moresco et al., *A 6% measurement of the hubble parameter at $z \sim 0.45$: direct evidence of the epoch of cosmic re-acceleration*, *Journal of Cosmology and Astroparticle Physics* **05** (2016) 014 [[1601.01701v2](#)].
- [105] F. Beutler et al., *The 6dF Galaxy Survey: $z \approx 0$ measurement of the growth rate and σ_8* , *Mon. Not. Roy. Astron. Soc.* **423** (2012) 3430 [[1204.4725](#)].
- [106] R. Tojeiro et al., *The clustering of galaxies in the SDSS-III Baryon Oscillation Spectroscopic Survey: measuring structure growth using passive galaxies*, *Mon. Not. Roy. Astron. Soc.* **424** (2012) 2339 [[1203.6565](#)].
- [107] S. de la Torre et al., *The VIMOS Public Extragalactic Redshift Survey (VIPERS). Galaxy clustering and redshift-space distortions at $z = 0.8$ in the first data release*, *Astron. Astrophys.* **557** (2013) A54 [[1303.2622](#)].
- [108] D. Stern, R. Jimenez, L. Verde, S.A. Stanford and M. Kamionkowski, *COSMIC CHRONOMETERS: CONSTRAINING THE EQUATION OF STATE OF DARK ENERGY. II. A SPECTROSCOPIC CATALOG OF RED GALAXIES IN GALAXY CLUSTERS*, *Astrophys. J. Suppl.* **188** (2010) 280 [[0907.3152](#)].
- [109] C. Chuang and Y. Wang, *Modeling the Anisotropic Two-Point Galaxy Correlation Function on Small Scales and Improved Measurements of $H(z)$, $D_A(z)$, and $f(z)\sigma_8(z)$ from the Sloan*

- Digital Sky Survey DR7 Luminous Red Galaxies*, *Mon. Not. Roy. Astron. Soc.* **435** (2013) 255 [[1209.0210](#)].
- [110] C. Blake et al., *Galaxy And Mass Assembly (GAMA): improved cosmic growth measurements using multiple tracers of large-scale structure*, *Mon. Not. Roy. Astron. Soc.* **436** (2013) 3089 [[1309.5556](#)].
- [111] A.G. Sanchez et al., *The clustering of galaxies in the SDSS-III Baryon Oscillation Spectroscopic Survey: cosmological implications of the full shape of the clustering wedges in the data release 10 and 11 galaxy samples*, *Mon. Not. Roy. Astron. Soc.* **440** (2014) 2692 [[1312.4854](#)].
- [112] S.N. Howlett et al., *The Clustering of the SDSS Main Galaxy Sample II: Mock galaxy catalogues and a measurement of the growth of structure from Redshift Space Distortions at $z = 0.15$* , *Mon. Not. Roy. Astron. Soc.* **449** (2015) 848 [[1409.3238](#)].
- [113] M. Feix, A. Nusser and E. Branchini, *Growth rate of cosmological perturbations at $z \sim 0.1$ from a new observational test*, *Phys. Rev. Lett.* **115** (2015) 011301 [[1503.05945](#)].
- [114] T. Okumura et al., *The Subaru FMOS galaxy redshift survey (fastsound). IV. New constraint on gravity theory from redshift space distortions at $z \sim 1.4$* , *Publ. Astron. Soc. Jap.* **68** (2016) 24 [[1511.08083](#)].
- [115] M. Moresco, *Raising the bar: new constraints on the Hubble parameter with cosmic chronometers at $z \sim 2$* , *Mon. Not. R. Astron. Soc.* **450** (2015) L16 [[1503.01116](#)].
- [116] C. Chuang et al., *The clustering of galaxies in the SDSS-III Baryon Oscillation Spectroscopic Survey: single-probe measurements from CMASS anisotropic galaxy clustering*, *Mon. Not. Roy. Astron. Soc.* **461** (2016) 3781 [[1312.4889](#)].
- [117] F. Beutler et al., *The clustering of galaxies in the completed SDSS-III Baryon Oscillation Spectroscopic Survey: Anisotropic galaxy clustering in Fourier-space*, *Mon. Not. Roy. Astron. Soc.* **466** (2017) 2242 [[1607.03150](#)].
- [118] N. Padmanabhan and M.J. White, *Constraining anisotropic baryon oscillations*, *Phys. Rev. D* **77** (2008) 123540 [[0804.0799](#)].
- [119] H. Gil-Marín et al., *The clustering of galaxies in the SDSS-III Baryon Oscillation Spectroscopic Survey: RSD measurement from the power spectrum and bispectrum of the DR12 BOSS galaxies*, *Mon. Not. Roy. Astron. Soc.* **465** (2017) 1757 [[1606.00439](#)].
- [120] A.J. Hawken et al., *The VIMOS Public Extragalactic Redshift Survey: Measuring the growth rate of structure around cosmic voids*, *Astron. Astrophys.* **607** (2017) A54 [[1611.07046](#)].
- [121] D. Huterer, D. Shafer, D. Scolnic and F. Schmidt, *Testing Λ CDM at the lowest redshifts with SN Ia and galaxy velocities*, *Journal of Cosmology and Astroparticle Physics* **05** (2017) 015 [[1611.09862](#)].
- [122] S. de la Torre et al., *The VIMOS Public Extragalactic Redshift Survey (VIPERS). Gravity test from the combination of redshift-space distortions and galaxy-galaxy lensing at $0.5 < z < 1.2$* , *Astron. Astrophys.* **608** (2017) A44 [[1612.05647](#)].
- [123] A. Pezzotta et al., *The VIMOS Public Extragalactic Redshift Survey (VIPERS): The growth of structures at $0.5 < z < 1.2$ from redshift-space distortions in the clustering of the PDR-2 final sample*, *Astron. Astrophys.* **604** (2017) A33 [[1612.05645](#)].
- [124] M. Feix, E. Branchini and A. Nusser, *Speed from light: growth rate and bulk flow at $z \sim 0.1$ from improved SDSS DR13 photometry*, *Mon. Not. Roy. Astron. Soc.* **468** (2017) 1420 [[1612.07809](#)].
- [125] C. Howlett et al., *2MTF VI. Measuring the velocity power spectrum*, *Mon. Not. Roy. Astron. Soc.* **471** (2017) 3135 [[1706.05130](#)].

- [126] F.G. Mohammad et al., *The VIMOS Public Extragalactic Redshift Survey (VIPERS): An unbiased estimate of the growth rate of structure at $\langle z \rangle = 0.85$ using the clustering of luminous blue galaxies*, *Astron. Astrophys.* **606** (2018) A59 [[1708.00026](#)].
- [127] Y. Wang et al., *The clustering of galaxies in the completed SDSS-III Baryon Oscillation Spectroscopic Survey: a tomographic analysis of structure growth and expansion rate from anisotropic galaxy clustering*, *Mon. Not. R. Astron. Soc.* **481** (2018) 3160 [[1709.05173](#)].
- [128] F. Shi et al., *Mapping the Real Space Distributions of Galaxies in SDSS DR7: II. Measuring the growth rate, clustering amplitude of matter and biases of galaxies at redshift 0.1*, *The Astrophysical Journal* **861** (2018) 137 [[1712.04163](#)].
- [129] H. Gil-Marín et al., *The clustering of the SDSS-IV extended Baryon Oscillation Spectroscopic Survey DR14 quasar sample: structure growth rate measurement from the anisotropic quasar power spectrum in the redshift range $0.8 < z < 2.2$* , *Mon. Not. Roy. Astron. Soc.* **477** (2018) 1604 [[1801.02689](#)].
- [130] J. Hou et al., *The clustering of the SDSS-IV extended Baryon Oscillation Spectroscopic Survey DR14 quasar sample: anisotropic clustering analysis in configuration-space*, *Mon. Not. Roy. Astron. Soc.* **480** (2018) 2521 [[1801.02656](#)].
- [131] G. Zhao et al., *The clustering of the SDSS-IV extended Baryon Oscillation Spectroscopic Survey DR14 quasar sample: a tomographic measurement of cosmic structure growth and expansion rate based on optimal redshift weights*, *Mon. Not. Roy. Astron. Soc.* **482** (2019) 3497 [[1801.03043](#)].

A RSD and OHD data tables

Index	Data set	z	$f\sigma_8(z)$	References	Index	z	H	References
1	SDSS-LRG	0.35	0.440 ± 0.050	[94]	1	0.0708	69.0 ± 19.68	[95]
2	VVDS	0.77	0.490 ± 0.18	[94]	2	0.09	69.0 ± 12.0	[76]
3	2dFGRS	0.17	0.510 ± 0.060	[94]	3	0.12	68.6 ± 26.2	[95]
4	2MRS	0.02	0.314 ± 0.048	[96, 97]	4	0.17	83.0 ± 8.0	[98]
5	SnIa+IRAS	0.02	0.398 ± 0.065	[97, 99]	5	0.179	75.0 ± 4.0	[100]
6	SDSS-LRG-200	0.25	0.3512 ± 0.0583	[101]	6	0.199	75.0 ± 5.0	[100]
7	SDSS-LRG-200	0.37	0.4602 ± 0.0378	[101]	7	0.20	72.9 ± 29.6	[95]
8	SDSS-LRG-60	0.25	0.3665 ± 0.0601	[101]	8	0.27	77.0 ± 14.0	[98]
9	SDSS-LRG-60	0.37	0.4031 ± 0.0586	[101]	9	0.28	88.8 ± 36.6	[95]
10	WiggleZ	0.44	0.413 ± 0.080	[102]	10	0.35	82.0 ± 4.85	[103]
11	WiggleZ	0.60	0.390 ± 0.063	[102]	11	0.352	83.0 ± 14.0	[104]
12	WiggleZ	0.73	0.437 ± 0.072	[102]	12	0.3802	83.0 ± 13.5	[104]
13	6dFGS	0.067	0.423 ± 0.055	[105]	13	0.4	95.0 ± 17.0	[98]
14	SDSS-BOSS	0.30	0.407 ± 0.055	[106]	14	0.4004	77.0 ± 10.2	[104]
15	SDSS-BOSS	0.40	0.419 ± 0.041	[106]	15	0.4247	87.1 ± 11.2	[104]
16	SDSS-BOSS	0.50	0.427 ± 0.043	[106]	16	0.4497	92.8 ± 12.9	[104]
17	SDSS-BOSS	0.60	0.433 ± 0.067	[106]	17	0.4783	80.9 ± 9.0	[104]
18	Vipers	0.80	0.470 ± 0.080	[107]	18	0.48	97.0 ± 62.0	[108]
19	SDSS-DR7-LRG	0.35	0.429 ± 0.089	[109]	19	0.593	104.0 ± 13.0	[100]
20	GAMA	0.18	0.360 ± 0.090	[110]	20	0.68	92.0 ± 8.0	[100]
21	GAMA	0.38	0.440 ± 0.060	[110]	21	0.781	105.0 ± 12.0	[100]
22	BOSS-LOWZ	0.32	0.384 ± 0.095	[111]	22	0.875	125.0 ± 17.0	[100]
23	SDSS DR10 and DR11	0.32	0.48 ± 0.10	[111]	23	0.88	90.0 ± 40.0	[108]
24	SDSS DR10 and DR11	0.57	0.417 ± 0.045	[111]	24	0.9	117.0 ± 23.0	[98]
25	SDSS-MGS	0.15	0.490 ± 0.145	[112]	25	1.037	154.0 ± 12.0	[100]
26	SDSS-veloc	0.10	0.370 ± 0.130	[113]	26	1.3	168.0 ± 17.0	[98]
27	FastSound	1.40	0.482 ± 0.116	[114]	27	1.363	160.0 ± 33.6	[115]
28	SDSS-CMASS	0.59	0.488 ± 0.060	[116]	28	1.43	177.0 ± 18.0	[98]
29	BOSS DR12	0.38	0.497 ± 0.045	[87]	29	1.53	140.0 ± 14.0	[98]
30	BOSS DR12	0.51	0.458 ± 0.038	[87]	30	1.75	202.0 ± 40.0	[98]
31	BOSS DR12	0.61	0.436 ± 0.034	[87]	31	1.965	186.5 ± 50.4	[115]
32	BOSS DR12	0.38	0.477 ± 0.051	[117]				
33	BOSS DR12	0.51	0.453 ± 0.050	[117]				
34	BOSS DR12	0.61	0.410 ± 0.044	[117]				
35	Vipers v7	0.76	0.440 ± 0.040	[118]				
36	Vipers v7	1.05	0.280 ± 0.080	[118]				
37	BOSS LOWZ	0.32	0.427 ± 0.056	[119]				
38	BOSS CMASS	0.57	0.426 ± 0.029	[119]				
39	Vipers	0.727	0.296 ± 0.0765	[120]				
40	6dFGS+SnIa	0.02	0.428 ± 0.0465	[121]				
41	Vipers	0.6	0.48 ± 0.12	[122]				
42	Vipers	0.86	0.48 ± 0.10	[122]				
43	Vipers PDR-2	0.60	0.550 ± 0.120	[123]				
44	Vipers PDR-2	0.86	0.400 ± 0.110	[123]				
45	SDSS DR13	0.1	0.48 ± 0.16	[124]				
46	2MTF	0.001	0.505 ± 0.085	[125]				
47	Vipers PDR-2	0.85	0.45 ± 0.11	[126]				
48	BOSS DR12	0.31	0.469 ± 0.098	[127]				
49	BOSS DR12	0.36	0.474 ± 0.097	[127]				
50	BOSS DR12	0.40	0.473 ± 0.086	[127]				
51	BOSS DR12	0.44	0.481 ± 0.076	[127]				
52	BOSS DR12	0.48	0.482 ± 0.067	[127]				
53	BOSS DR12	0.52	0.488 ± 0.065	[127]				
54	BOSS DR12	0.56	0.482 ± 0.067	[127]				
55	BOSS DR12	0.59	0.481 ± 0.066	[127]				
56	BOSS DR12	0.64	0.486 ± 0.070	[127]				
57	SDSS DR7	0.1	0.376 ± 0.038	[128]				
58	SDSS-IV	1.52	0.420 ± 0.076	[129]				
59	SDSS-IV	1.52	0.396 ± 0.079	[130]				
60	SDSS-IV	0.978	0.379 ± 0.176	[131]				
61	SDSS-IV	1.23	0.385 ± 0.099	[131]				
62	SDSS-IV	1.526	0.342 ± 0.070	[131]				
63	SDSS-IV	1.944	0.364 ± 0.106	[131]				